Composite detectors based on SCF and single crystals of garnet compounds

Sandra Witkiewicz-Lukaszek[1], Vitalii Gorbenko[1], Tetiana Zorenko[1], Yurii Syrotych[1], Jiri A. Mares[2], Martin Nikl[2], Oleg Sidletskiy[1,3,4], Pawel Bilski[5] , Akira Yoshikawa[6] and Yuriy Zorenko[1]*

[1]Institute of Physics, Kazimierz Wielki University in Bydgoszcz, Powstańców Wielkopolskich str., 2, 85090 Bydgoszcz, Poland; e-mail: *s-witkiewicz@wp.pl; gorbenko@ukw.edu.pl; tzorenko@ukw.edu.pl, syr@ukw.edu.pl, zorenko@ukw.edu.pl*

[2]Institute of Physics, Academy of Sciences of Czech Republic, Cukrovarnicka str., 10, 16200 Prague, Czech Republic; e-mail: *amares@fzu.pl; nikl@fzu.pl*

[3] Institute for Scintillation Materials, National Academy of Sciences of Ukraine, 61072 Kharkiv, Ukraine; e-mail: *sidletskiy@isma.kharkov.ua*

[4]Centre of Excellence ENSEMBLE3 Sp. z o.o., ul. Wolczynska 133, 01-919 Warsaw, Poland; e-mail: *oleg.sidletskiy@ensemble3.eu*

[5]Institute of Nuclear Physics, Polish Academy of Sciences, Krakow, Poland; e-mail: *pawel.bilski@ifj.edu.pl*

[6] Institute for Materials Research, Tohoku University, 2-1-1 Katahira, Aoba-ku, Sendai 980-8577, Japan; e-mail: *yoshikawa@imr.tohoku.ac.jp*

* Correspondence: *zorenko@ukw.edu.pl*

Abstract: This manuscript summarizes last results on the development of composite luminescent materials based on the SCF and single crystals of simple and mixed garnet compounds obtained by the liquid-phase epitaxy growth method. Such composite materials can be applied as scintillating and thermoluminescent (TL) detectors for radiation monitoring of the mixed ionization fluxes, as well as the scintillation screens in the microimaging techniques. The film and crystal parts of composite detectors were fabricated from efficient scintillation / TL materials based on Ce^{3+}, Pr^{3+} and Sc^{3+} doped $Lu_3Al_5O_{12}$ garnets, as well as Ce^{3+} doped $Gd_{3-x}A_xAl_{5-y}Ga_yO_{12}$ mixed garnets, where A = Lu or Tb; x = 0-1; y = 2-3 with significantly different scintillation decay or positions of the main peaks in their TL glow curves. This work also summarizes the results of optical study of films, crystals and epitaxial structures of these garnet compounds using absorption, cathodoluminescence and photoluminescence. The scintillation and TL properties of the developed materials under α- and β - particles and□□□□quanta excitations were studied as well. The most efficient variants of the composite scintillation and TL detectors for monitoring of composition of mixed beams of ionizing radiation were selected based on the results of this complex study.

Keywords: scintillators; thermoluminescence, substrates; crystals, SCF; composite detectors; liquid-phase epitaxy

1. Introduction

The technology of the liquid phase epitaxy (LPE) developed over last 30 years offers a possibility of creating luminescent materials on the base of single crystalline films (SCF) of complex oxides [1-3] for application in cathodoluminescent screens [4, 5, 6], laser media [7, 8], scintillators for registration of α– and β–particles, X-ray or γ-quanta [1, 9, 10] and scintillating screens for microtomography detectors employing X-ray sources and synchrotron radiation [11, 12].

Furthermore, advanced composite scintillators (CS) [1, 9, 13-22] and thermoluminescent (TL) detectors [23-26] of "phoswich-type" (phosphor sandwich) may be fabricated by the LPE method for simultaneous registration of different components of ionizing radiation, namely, for content analysis of the mixed radiation fluxes involving ionizing particles with various penetration depths. These CS and detectors comprise epitaxial crystalline structures, including one/two SCFs for registration of low-penetrating α- and β-particles, and bulk single crystal (SC) substrates for registration of the high-penetrating radiation (X or γ rays) (Fig. 1).

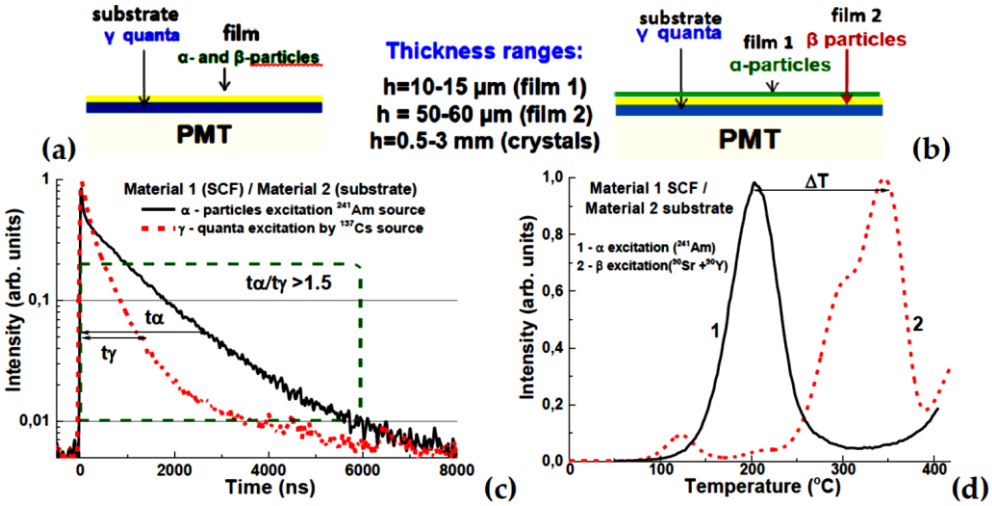

Fig. 1. Scheme of a two-layer (a) and three-layer (b) composite scintillator or TL material, (c) - example of the scintillation decay of the film and substrate parts of composite scintillator at registration of α- particles and γ- quanta [14], (d) - example of recording ΔT temperature difference between the main peaks in TL glow curves of the film and substrate in a composite TL material [25,26].

Composite scintillator and detectors: fundamentals

The following considerations should be taken into account at development of the CS. The signals from a substrate registering a high penetrating component of ionizing particles and film registering a low-penetrating

component must be distinguished as clear as possible by luminescence band spectral composition and/or luminescence decay time (Fig.1a). At the same time, decay times should be fast enough for compatibility with fast operation devices, typically within 1000 ns. Furthermore, light outputs of both film and substrates should be as high and possible to enhance the registration efficiency. A substrate should efficiently absorb as much as possible high-penetrating particles and transmit low-penetrating particles, whereas the opposite is expected from a film. The ideal situation represents a thick enough substrate comprising a high density (high Z_{eff}) material, and thin enough (or low density/low Z_{eff}) film transmitting a high-penetrating component. The limitations on the materials used in CS include the misfit between a substrate and film lattice parameters, which should not exceed typically 1 – 1.3 % in the case of garnets [27-29], and the component cost, which should be as low as possible by avoiding or minimizing consumption of the expensive components such as Lu_2O_3 and Ga_2O_3. Furthermore, a substrate should be transparent to luminescence of a film if a photodetector is located under the substrate.

Thermoluminescence (TL) is also a well-established method of radiation dosimetry, widely used in radiation protection and medical applications [30, 31]. Unlike scintillation, it is a passive integrating technique, in which the measurement of the absorbed dose ('reading' of a TL detector) is performed some time (often long) after the actual exposure. The most common of TL detectors are these based on lithium fluoride [33], but new materials and new applications are still under development [34]. In the past, some types of thin film TL detectors for measurements of weakly penetrating radiation [35-39] have been developed. Recently, we have also studied the possibility of using LPE-grown SCFs of oxide compounds (perovskites, garnets, orthosilicates) for this purpose [23-26, 39]. Furthermore, the combination of these materials can be considered as well in frame of development of composite two-layered epitaxial structures capable to register components in mixed radiation beams (Fig.1b).

Garnets hosts were chosen for development of composites due to their relatively easy growth process in both bulk and film forms. The cubic structure of garnet implies fewer limitations on the film orientation. If to consider just "simple" rare earth garnets, the heaviest $Lu_3Al_5O_{12}$ (LuAG) host should be chosen as a substrate [13-18, 40-44], while the film should comprise lighter $Y_3Al_5O_{12}$ (YAG) -based compositions [1, 9, 13]. The luminescence signals from LuAG and YAG can be distinguished by doping them with different activators having various luminescence lifetimes, such as Pr^{3+} (15-25 ns), Ce^{3+} (40-70 ns), Sc^{3+} (245-610 ns) in garnet hosts [15, 16, 40-44], or using the property of faster luminescence decay in films than that in bulk crystals with the same composition due to lower quantity of defects in the former.

Meanwhile, new prospects in engineering of the garnet CS have been opened with the development of the bulk crystals of mixed $(Lu,Gd,Tb)_3(Al,Ga)_5O_{12}$ garnets possessing much higher light output even over 50 000 photon/MeV [43-45]. Nowadays Ce-doped mixed garnets are among the most extensively developed garnet scintillators [43-55]. The focus of the recent studies was concentrated on mixed systems with the first

(Lu,Gd,Tb) and second (Al,Ga) cation substitutions (Fig. 2a). An effect of a nonlinear decrease in the conduction and valence band minima

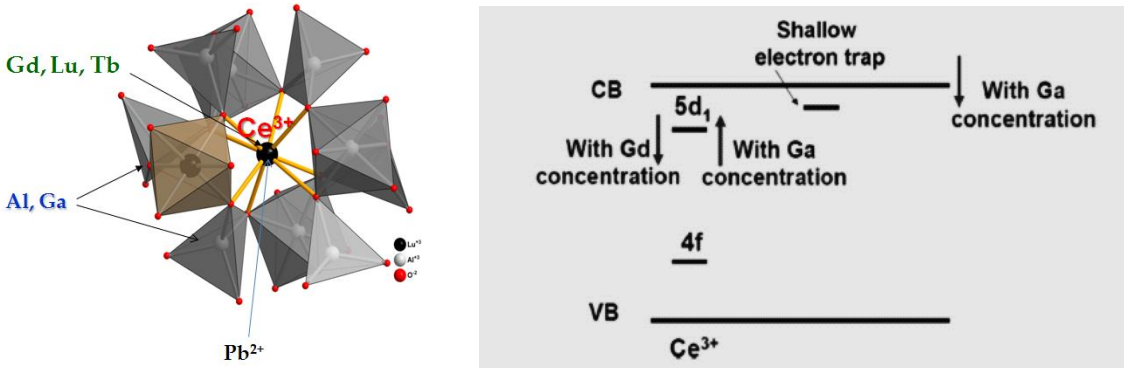

Fig. 2. (a) - structure of the garnet crystal lattice showing the crystallographic sites occupied by different cations [56]; (b) – shifts of $5d_1$ energy level of Ce^{3+} ions in $Lu_{3-x}Gd_xAl_{5-y}Ga_yO_{12}$:Ce garnet caused by variations of x and y (CB, VB – conductive and valence bands, respectively) [57, 58].

relatively to the vacuum referred binding energy with Ga doping in$(Lu,Gd,Tb)_3(Al,Ga)_5O_{12}$ garnets was studied in details [43, 46]. The change matrix composition affects also on the characteristics of Ce^{3+} emission in mixed garnets [43, 46, 47]. Generally, the substitution of Lu^{3+} cations by the large R = Gd^{3+} or Tb^{3+} ions in the $(Lu_xR_{1-x})_3Al_{5-y}$ Ga_yO_{12}:Ce lattice results in an red emission shift and in increase splitting of the lowest doublet 5d state of Ce^{3+} with respect to conduction band bottom (Fig.2b), as well as in changing the rates of intra-center and extra-center energy relaxation to Ce^{3+} emitting ions [48, 50]. Finally, the of such double cation substitutions leads to strong increasing LY mixed garnet scintillators with respect to “simple” LuAG:Ce and YAG:Ce garnets [43, 50, 55].

Furthermore, isomorphic cation substitution in mixed garnets provides also the possibility of precise tuning of lattice parameters of SCF scintillators to reduce a mismatch between films and substrates [59, 60]. First of all, we considered combinations of the bulk crystals $(Gd,Lu)_3(Al,Ga)_5O_{12}$ (GAGG:Ce) scintillators possessing an extremely high light yield and their SCF counterparts [62-66]. Performances of GAGG:Ce substrates and films with varying Al/Ga ratios were explored [62-66]. Finally, the experiments on Lu/Tb/Gd and Al/Ga substitutions were conducted to achieve the best optimal and scintillation performance of the CS [67-69].

CS and detectors: history and perspective

The first CS created back in 1990 were based on the LPE-grown $Y_3Al_5O_{12}$ (YAG) epitaxial structures [1, 9, 13, 14]. Double-layered YAG:Ce SCF/YAG:Nd SC and YAG:Ce SCF / YAG:Sc SC structures, as well as triply-layered CS of YAG:Ce SCF / YAG:Nd SCF /YAG:Sc SC structure were LPE-grown and tested under excitations by α- or β- particles and γ-quanta [1, 9, 13]. The scintillation signals emitted by the SCF and SC parts of CS were distinguished using the differences in their scintillation decay [1, 9, 13].

Regarding the radiation monitoring, scintillators with a low density ρ=4.57 g/cm^3 and effective atomic number Z_{eff} = 29 based on the YAG SCs were mainly used for low-energy radiation monitoring [1, 9, 13]. Therefore, garnet CS with high ρ and Z_{eff} values were demanded for minoroting of mixed fluxes of α- or β-particles and high-energy γ- quanta [14] (Table 1).

$Lu_3Al_5O_{12}$ garnet (LuAG) is the most obvious candidate among heavy garnets [11, 40-44] with a higher density ρ= 6.73 g/cm^3 and Z_{eff}=61 as compared to YAG (Table 1). LuAG:Ce, LuAG:Pr and LuAG:Sc are well-known scintillators [42, 43], while Ce^{3+}, Pr^{3+} and Sc^{3+} ions are the most efficient activators in

Table. 1. Selected properties of materials for garnet CS. The data were collected from the producer websites [40-44] (literature data in brackets may differ from the data provided by producers).

Parameter	YAG:Ce	LuAG:Ce	LuAG:Pr	LuAG:Sc	GAGG:Ce
Density [g/cm^3]	4.57	6.73	6.73	6.73	6.63
Effective atomic number	74	58.9	62.9	61	54.4
Wavelength of max. emission [nm]	550	535	310	280	520
Decay constant [ns]	70	70	20(19-28)	245-610	50-150
Photon yield [ph/MeV]	30*10^3	25*10^3	15-18*10^3	22.5*10^3	40-60*10^3
LY_α/LY_γ in the range 0.5-10 μs		0.1-145	0.31-0.34	0.38-0.42	0.19-0.2
Energy resolution [%]	6.7	5.5-7	<5	7	6.68

garnet hosts with the different luminescence decay [3, 40-44]. It was shown [12, 40-44] that the LY of Ce^{3+}, Pr^{3+} and Sc^{3+} doped LuAG crystals and SCFs exceed those of YAG-based counterparts (Table 1). This became an additional argument for the production of a new generation of high-performance CS based on LuAG crystals and films [15-19].

Composition engineering of the cation content [42] and bang gap engineering of garnet compounds became a novel approach for development of scintillation materials [57] (Fig. 2), opening new avenues for the creation of advanced CS. Bulk SCs of $Gd_3Al_{5-x}Ga_xO_{12}$ garnets at x=2-3 are now among the mosy on the top list of scintillators with a very high light yield (LY) of up to 50 000 Photons/MeV under excitation by γ quanta of ^{137}Cs (662 keV) source [42-45]. The solid solutions of $Lu_{3-x}Gd_xAl_{5-y}Ga_yO_{12}$ mixed garnets at x=1-3; y=2-3 are also very promising materials for creation of the SCF scintillation screens with high absorption ability for X-rays and a very high efficiency of the of α-particles registration [61-65].

Scintillators in the form of LGAGG:Ce SCFs due to a larger lattice constant can also be crystallized on both YAG and GAGG substrates [61-65]. Furthermore, a successive crystallization of TbAG:Ce SCFs onto undoped GAGG substrates [66-69], confirmed the possibility of crystallization of good quality SCF scintillators even in the case of a large (up to 1.3%) misfit between SCF and SC lattices. Following this progress, it

seemed reasonable developing new types of CS for radiation monitoring by combining GAGG:Ce crystals and LGAGG:Ce or TbAG:Ce SCFs into one composite material [20-22]. Hence we developed a novel *approach to the creation of CS based* on *the combination of different scintillation material hosts doped with the same activator (Ce^{3+}).*

Finally, the last part of this review demonstrates the possibility of *developing composite TL detectors based on garnet epitaxial structures.* Among possible compounds, YAG:Ce and LuAG:Ce crystals and SCFs of these garnets, as well as $Lu_{3-x}Gd_xAl_5O_{12}$:Ce SCFs were considered [23, 24]. The operation principle of such composite TL materials is based on differences in temperatures of main peaks in glow curves corresponding to SCF and SC components under excitation with α or β particles (Fig.1b). Therefore, developed garnet epitaxial structures can be considered *as prototypes* of composite TL detectors.

Following the achievements mentioned above the main goal of our recent activities was crystallization by the LPE method and study of luminescent, scintillation and TL properties of composite materials based on "film-crystal" epitaxial structures of simple and mixed garnets for monitoring of mixed ionization fluxes in the *active* and *passive* modes based on the scintillation and thermoluminescence phenomena, respectively.

2. Materials and Methods

2.1. Crystallization of scintillation films by LPE method

CS based on garnet crystals and films (Fig. 3) were grown by the LPE method in Epitaxy Laboratory of Chair for Optoelectronic Materials in Institute of Physics of Kazimierz Wielki University (UKW) in Bydgoszcz, Poland. Substrates for film deposition were produced by Institute for Scintillation Materials (ISMA), Kharkiv, Ukraine (LuAG:Ce, LuAG:Sc, GAGG:Ce), CRYTUR Ltd company, Czech Republic (LuAG:Pr), and Institute for Materials Research (IMR), Tohoku University, Sendai, Japan (GAGG:Ce).

The LPE method provides crystallization of SCF of different oxide compounds with a very good structure and optical quality with the prescribed thickness. Such method is based on creation of oversaturation of crystallized substance in solution making it possible to grow films at relatively low temperatures of approximately 1000 °C compared with crystallization conditions at growth of the same materials from the melt at temperatures around 2000 °C.

The charge for the film crystallization is prepared by mixing raw materials containing the film-forming cations in appropriate proportions. In order to calculate the amount of individual elements needed to obtain the final product, it is necessary to know the molar mass of the raw material, from which this element can be selected in the respective proportion.

A standard purity of raw material components was not less than 99.99 %. During the preparation of the charge for the production of thin SCFs using the LPE method, the so-called Blank-Nielsen coefficients R_1, R_2, R_3 i R_4 should be maintained corresponding to the ratios

$$R_1 = \frac{P_{flux_{PbO}}}{P_{flux_{B2O3}}}; R_2 = \frac{\sum P_{garnet(dod)}}{\sum P_{garnet(oct+tet)}}; \quad R_3 = \frac{\sum P_{garnet}}{\sum P_{garnet}+\sum P_{flux}}; ; \; R_4 = \frac{\sum P_{dopant}}{\sum P_{garnet}},$$

where *P* are mole weights of the PbO and B_2O_3 flux components as well as garnet and activator host components occupying dodecahedral (dod), octahedral (oct) and tetrahedral (tet) positions in the garnet lattice, respectively.

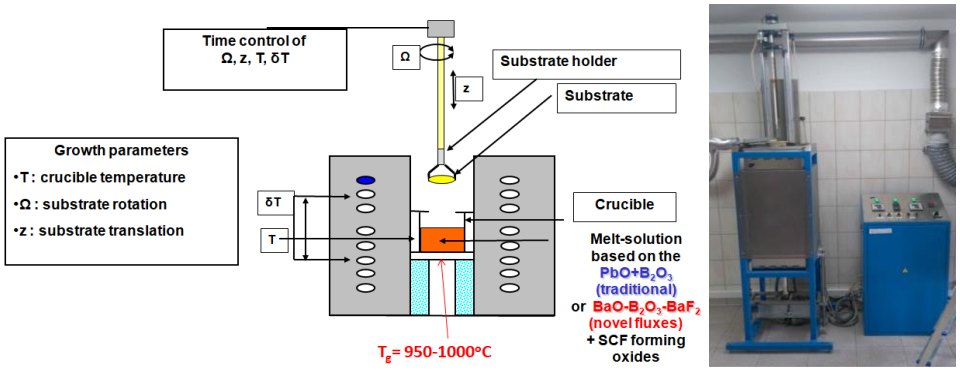

Fig. 3. Scheme and photo of the setup for growth of SCF by the LPE method at Chair of Optoelectronic Materials in Institute of Physics of University of Kazimierz Wielki in Bydgoszcz.

The ratio R_1=11-12 determines kinetic characteristics of the solution and the solubility of the oxides constituting the film. R_2 = 0.02-0.035 corresponds to the garnet phase as the main phase at the film crystallization. Meanwhile, the choice of R_3 and R_4 in the ranges of 0.02-0.035 and 0.01-0.15, respectively, relates to the optimization of a film scintillation efficiency.

The charge was dissolved in a mix of lead oxide PbO and boron oxide B_2O_3 in the ratio of 88-90%: 10-12% which was typically used as a flux. The molar concentration of the flux in the solution expressed by the R_3 coefficient was 95% -97%. Flux components, in particular, divalent lead ions Pb^{2+} and tetravalent Pb^{4+} ions, may also incorporate the films and give rise to undesirable effects. Lead admixture strongly reduces the luminescence efficiency of activators such as Ce^{3+}, Pr^{3+} and Sc^{3+}. On the other hand, solutions of PbO and B_2O_3 are characterized by a very good solubility of film-forming materials, relatively low viscosity and high fluidity that is highly important during crystallization of films with a high structural and optical quality.

The prepared raw materials with the composition meeting the specified R_1 - R_4 values were placed in Pt crucibles of a 30-40 mm diameter. The crucible material was chosen accounting for a high melting temperature of 1768 ˚C and weak impact of Pt admixture on optical quality of films.

The basic mechanism determining the formation of a single crystalline film onto the substrate is the process of *supercooling the solution*. For this purpose, a crucible is placed in a furnace (Fig. 3) and heated to a temperature of 1050-1100˚C. At this temperature, the melted materials form an unsaturated solution characterized by a certain saturation temperature T_S (*solidus temperature*), which is a function of the R_3 coefficient.

As solution temperature is lowered below T_S to growth temperature T_g in the 950-1050 ˚C range, the solution undercools, and the excess solute deposits on the rotating substrate introduced into the solution.

The substrate dimensions should not exceed half of the crucible diameter, i.e. 15-20 mm. The SCF growth rate of depends on several factors, mainly the difference ΔT between growth temperature T_g and melt saturation temperature T_S. In general, the film thickness is proportional to the degree of supercooling $\Delta T = T_g - T_S$, and the square root of the substrate rotation rate ω. The obtained SCF scintillators typically had the thickness in the 15-50 μm range. The LPE growth of SCFs of multi-component mixed garnets, in general, is complicated due to chemical complexity and specific segregation phenomena for different types of cations [59-65]. For this reason, typically the actual SCF composition differs with respect to the nominal melt-solution composition.

2.2. Characterization of CS and TL detectors

The actual compositions of single crystals and films was determined using a JEOL JSM-820 electronic microscope equipped with an IXRF 500 i LN2 Eumex EDX detectors. Structural quality of SCFs with different content, as well as the SCF/substrate misfit $\mathbf{m} = [(\mathbf{a_f} - \mathbf{a_{sub}})/ \mathbf{a_{sub}}]*100$ % between the lattice constant of SCF $\mathbf{a_f}$ and substrate $\mathbf{a_{sub}}$. Were determined from XRD patterns (spectrometer DRON 4, X-ray source).

Absorption spectra, cathodoluminescence (CL) spectra, light yield (LY) and scintillation decay kinetics were measured under excitation by α–particles from ^{239}Pu (5.15 MeV) and ^{241}Am (5.5 MeV) sources as well as ^{137}Cs (662 keV) source, respectively. $Gd_3Al_{2.5}Ga_{2.5}O_{12}$:Ce (GAGG2.5:Ce) and Gd_3Al_2 Ga_3O_{12} :Ce (GAGG3:Ce) crystals with the size of 5∗5∗0.9 mm produced in ISMA, Ukraine and IMR Tohoku University, Japan, as well as YAG:Ce SCF were used as reference samples at CS characterization. The absorption spectra were registered using a Jasco 760 UV-Vis spectrometer in the 200-1100 nm range. The CL spectra were registered at room temperature (RT) using a SEM JEOL JSM-820 electron microscope equipped with a Stellar Net spectrometer and TE-cooled CCD detector working in the 200-925 nm range. The scintillation LY determined from pulse height spectra (PHS) recorded with a shaping time of 12 □s was registered using a setup based on a Hamamatsu H6521 photomultiplier (PMT), multi-channel analyzer and a Tektronix TDS3052 digital oscilloscope under excitation by α-particle of ^{239}Pu (5.15 MeV) source. The spectra were calibrated with a standard YAG:Ce SCF sample with a photoelectron yield of 360 phels/MeV and LY of 2650 photons/MeV.

Scintillation response of CS was determined using the set-up consisting of a hybrid PMT (HPMT DEP PP0475B), controlled by PC. PHS were registered under excitation with α-particles with the energy of 5.4857 MeV of ^{241}Am radioisotope and with γ-rays of ^{137}Cs (energy 661.66 keV) radioisotope. Herein, α-particles of ^{239}Pu and ^{241}Am sources excite only epitaxial layers of SCF samples (not their substrates), because α-particle penetration depth in the studied materials is approximately 12-15 μm.

TL glow curves were measured under the excitation by α- and β-particles from ^{241}Am and ^{90}Sr + ^{90}Y sources using a Risø TL/OSL-DA-20 reader (Risø DTU, Roskilde, Denmark). A “green” Schott BG 39 filter

was used for the registration of TL signal. The filter transmittance range of 350 to 700 nm matched well with the Ce^{3+} emission range.

3. Results

3.1. CS based on LuAG substrates doped with Pr, Sc and Ce ions

3.1.1. Substrates based on LuAG crystals.

In the first phase of CS development, it is very important to analyze the scintillation decay curves of Ce^{3+}, Pr^{3+} and Sc^{3+}-doped LuAG substrates under excitation with □□particles and □□quanta. This analysis was performed on 1 mm thick substrates (Fig. 4).

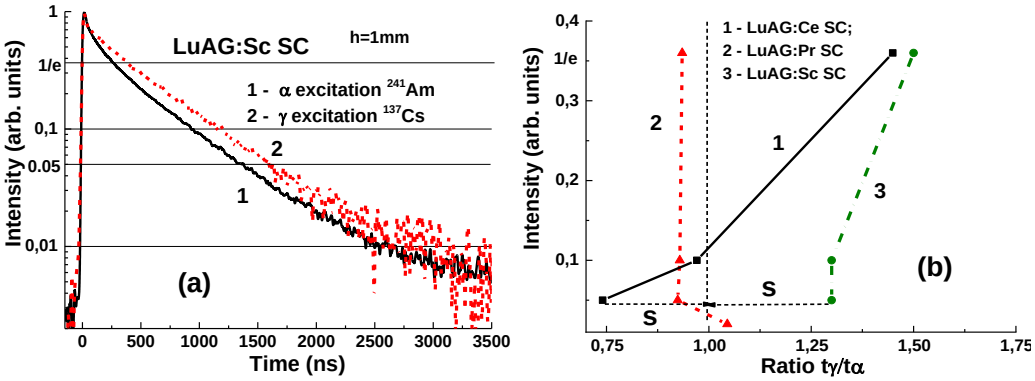

Fig. 4. (a) – scintillation decay kinetics of LuAG:Sc substrate under with α-particle (1) and γ quanta excitation (2); (b) t_γ/t_α ratio at different luminescence intensities for LuAG:Ce (1), LuAG: Pr (2) and LuAG:Sc (3) substrates [27].

The various scintillation decays for the mentioned substrates are illustrated by Fig. 4a. Slightly larger difference is observed for the LuAG:Ce and LuAG:Sc substrates, which can be quantified by the t_γ/t_α ratio reaching 1.45 and 1.5, respectively, on the 1/e level.

3.1.2. CS based on a LuAG:Ce

LuAG:Pr SCF/LuAG:Ce and LuAG:Sc SCF/LuAG:Ce CS were developed in [15,16]. Features of α-particles and □- quanta interaction with the mentioned materials cause a big difference in scintillation efficiency at their registration, expressed by the ratio LY_α/LY_γ. Fig. 5 shows PHS of these CS under excitation by α-particles and □-quanta. The main peak in Fig. 5a corresponds to the full absorption of α-particles with a 5.5 MeV energy, while the left peak is associated with the absorption of □ quanta of a ^{137}Cs source with an energy of 59.65 keV. It is important that the positions of the peaks corresponding to α-particles excitation of LuAG:Pr and LuAG:Sc SCFs are different from those for the LuAG:Ce SC substrate (Fig. 5a). This means that α-particles are registered only by the SCF and do not excite the substrate.

At excitation of LuAG:Pr SCF/LuAG:Ce SC and LuAG:Sc SCF/LuAG:Ce CS by γ-quanta from ^{137}Cs source, the additional and main peaks in the amplitude spectra correspond to the total absorption of γ-rays with

the 32 keV and 662 keV energies (Fig. 5b). It is important that the main photopeaks of LuAG:Ce SC and CS in Fig. 5b have a similar position certifying full absorption of γ-quanta in the substrate parts of such composites.

The remarkable differences in the scintillation decay of LuAG:Pr SCF/LuAG:Ce SC and LuAG:Sc SCF/LuAG:Ce CS are observed under γ-rays and α–particles with a t_α/t_γ value ranging within 0.27–0.35 and 1.1–2.2, respectively, at luminescence intensity decay from 1/e down to 0.05 (Fig. 6c) [15, 16].

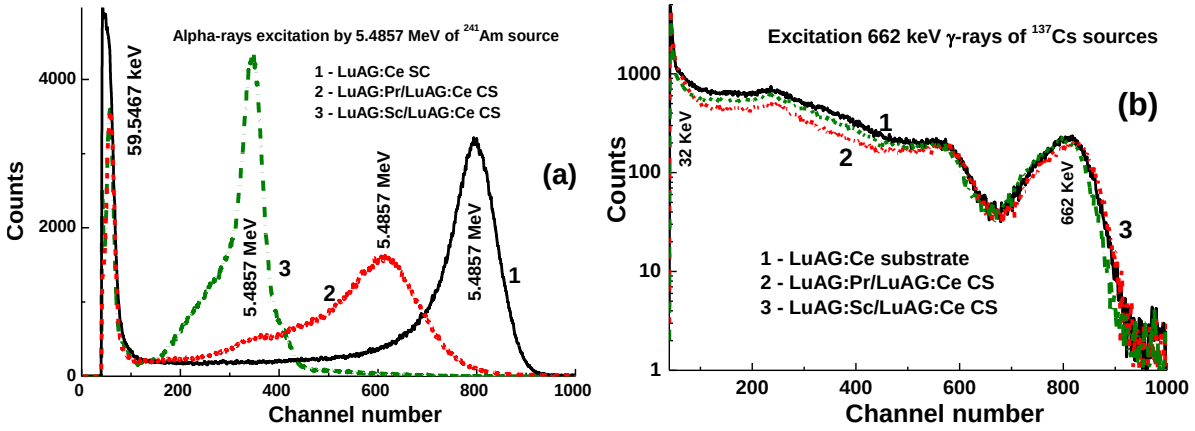

Fig. 5. PHS of LuAG:Ce SC substrate (1), LuAG:Pr SCF/LuAG:Ce SC (2), LuAG:Sc SCF/LuAG:Ce SC (3) CS under α-particles and γ- quanta excitations [15,16].

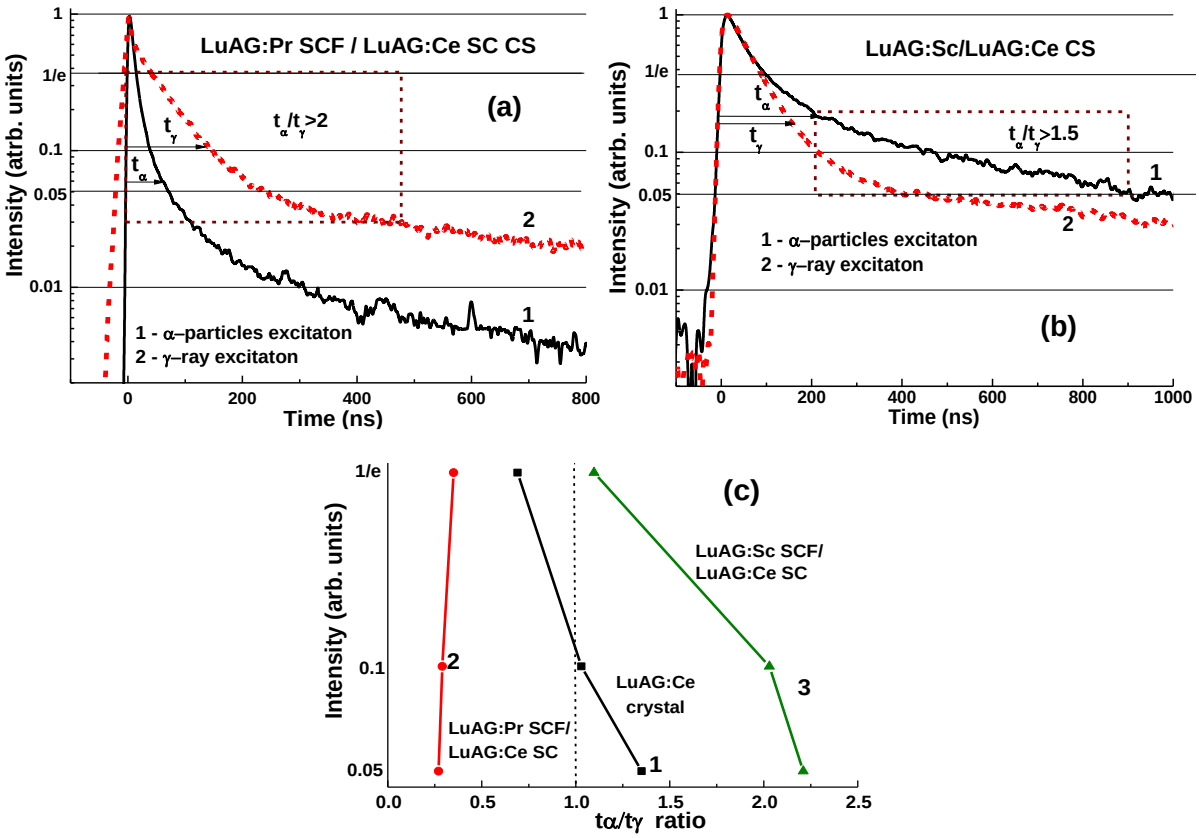

Fig. 6. Scintillation decay kinetics of LuAG:Pr SCF / LuAG:Ce SC (a) and LuAG:Sc SCF / LuAG:Ce SC (b) CS under excitation by α-particles (1) and γ-quanta (2). (c) - t_γ/t_α ratio for different levels of scintillation decay for these CS (1, 2) compared to the LuAG: Ce substrate (3) [15,16].

A LuAG:Pr SCF/LuAG:Ce SC composite scintillator has a certain advantage over LuAG:Sc SCF/LuAG:Ce SC composition due to a larger $t_{\alpha/\gamma}$ ratio in the entire 0 - 700 ns time range (Fig. 6a). However, LuAG:Sc SCF/LuAG:Ce SC composite scintillator separates the scintillation signals from the SCF and the substrate even with a better t_{α}/t_{γ} ratio, but in the narrow time interval of 200 - 900 ns and in a smaller intensity range between 0.2 and 0.05 (Fig. 6c). Meanwhile, these results prove that both types of CS are capable to distinguish α-particles and γ-quanta in mixed fluxes.

3.1.3. CS based on LuAG:Pr substrate

This subsection is focused on the development of CS based on the LuAG:Pr SC and SCF of $Lu_{2-x}GdTb_xAl_5O_{12}$:Ce and $Lu_{3-x}Tb_xAG$:Ce mixed garnets with an *x* ranged within 0.15-2.285. Adjusting the cation ratio in the garnet compositions provides favorable changes in scintillation properties of CS [17].

Amplitude spectra of LuAG:Ce SCF/LuAG:Pr SC, $Lu_{2.85}Tb_{0.15}AG$:Ce SCF / LuAG:Pr SC and $Lu_{1.7}GdTb_{0.3}AG$:Ce SCF / LuAG:Pr SC CS for the registration of α- particles and □□quanta are presented in Fig. 7. Different

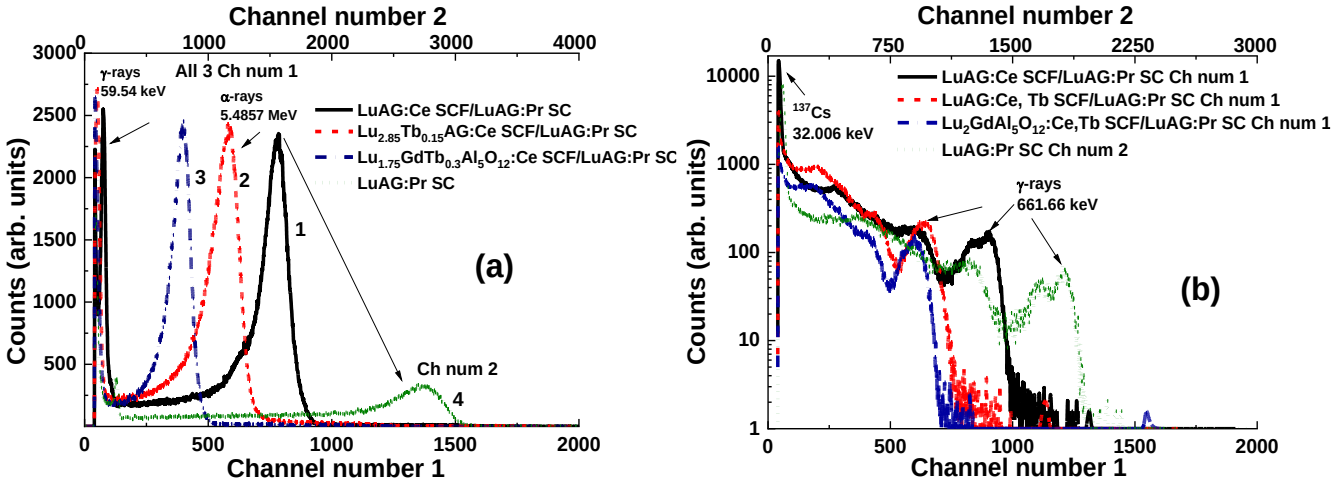

Fig. 7. PHS of LuAG:Ce SCF/LuAG:Pr SC (1), $Lu_{2.85}Tb_{0.15}AG$:Ce SCF/LuAG:Pr SC (2), $Lu_{1.7}GdTb_{0.3}AG$:Ce SCF/ LuAG:Pr SC (3) CS and LuAG:Pr SC (4) under excitation with α-particles (a) and γ-quanta (b) [17].

locations of the SCFs main peaks in the mentioned CS compared to the LuAG:Pr substrate indicate that α-particles excite only the SCF part of the composite scintillator. The same situation is observed under excitation of the mentioned composites with γ-quanta (Fig. 7b). The SCF main peak location depends on the type, thickness and LY of CS (Fig. 7a) and evidences the significant impact of LuAG-based SCF to the γ-ray absorption.

The best separation of the decay curves from the LuAG:Pr substrate and $Lu_{3-x}Tb_xAG$:Ce SCF at x = 0.15-0.3 was achieved at high concentration of Tb^{3+} cations (x = 1.65-2.285). For comparison, the scintillating decay

times of $Lu_{3-x}Tb_xAG:Ce$ (x=0.64; 1.05 and 2.15) SCFs scintillators grown onto LuAG:Pr substrates were compared under α-particles and ɣ-ray excitations. Crystallization of the latter, however, was associated with a high mismatch of crystal lattices above 1%.

Following the successful crystallization of $Lu_{3-x}Tb_xAG:Ce$ SCF with Tb x = 0.65-2.285 onto LuAG:Pr substrates, remarkably better t_γ/t_α value were obtained in the CS with high Tb concentrations (Fig. 8b). An example of a good separation of the decay curves at excitation of the $Lu_{0.715}Tb_{2.285}AG:Ce$ SCF /LuAG:Pr SC composite scintillator with α particles and γ quanta presented in Fig. 8a demonstrates the t_α/t_γ ratios in the range of 1.56-4.16 as the luminescence decays from 1/e to 0.1 (Fig. 8b).

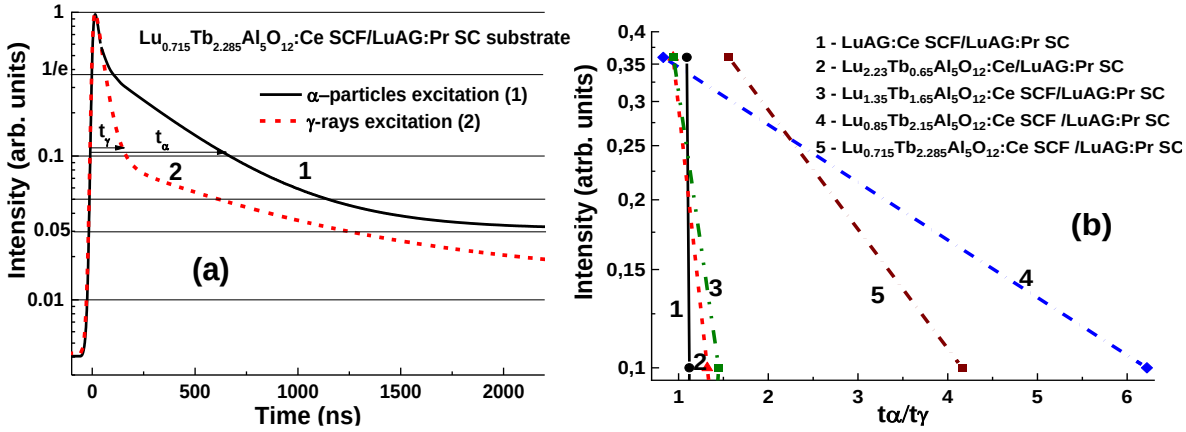

Fig. 8. (a) – Scintillation decay of $Lu_{0.715}Tb_{2.285}Al_5O_{12}$:Ce SCF/LuAG:Pr SC composite scintillator (b) under excitation by α-particles (1) and γ quanta (2). (b) - tγ/tα ratios for the different levels of luminescence intensity decrease for $Lu_{3-x}Tb_xAl_5O_{12}$:Ce SCF/LuAG:Pr SC CS with the Tb content x = 0 (1), 0.65 (2), 1.65 (3), 2.15 (3) and 2.285 (4) [17].

3.1.4. CS based on LuAG:Sc substrate

The last set of CS based on LuAG epitaxial structures are LuAG:Ce and LuAG:Pr SCFs with the 12-30 μm thickness based on LuAG:Sc substrates [18, 19]. PHS of these CS under excitation by α-particles and quanta are presented in Fig. 9. It is noteworthy that at registration of α-particles the main peaks are shifted relatively to each other and to the substrate (Fig. 9a), because α-particles excite only the film part of CS. At registration of γ-quanta, the main peaks are also shifted (Fig. 9b) indicating the excitation of both the substrate and SCF. Therefore, the total absorption of 662 keV γ-quanta also depends on the type, thickness and LY of the SCF affecting scintillation properties of the entire CS.

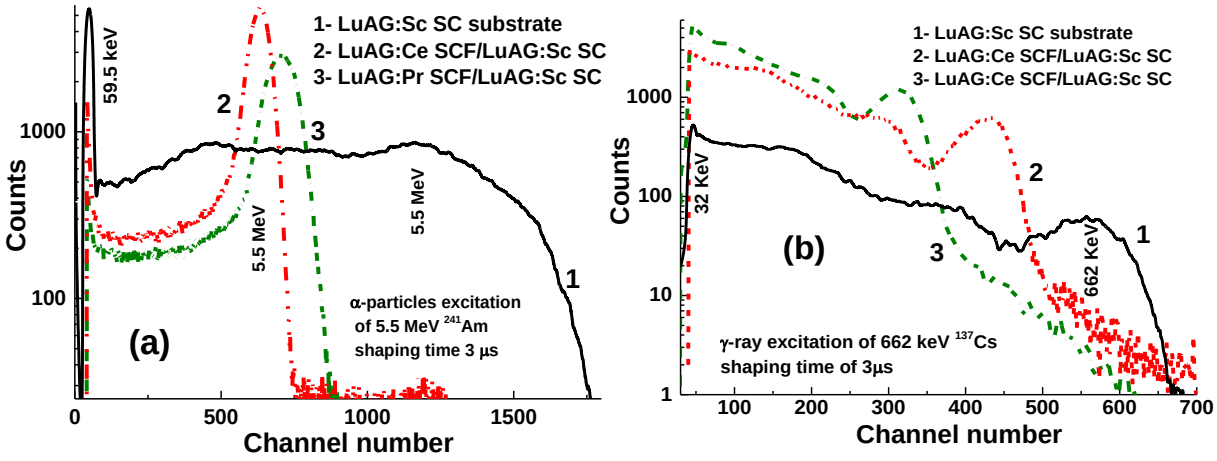

Fig. 9. Pulse height spectra of LuAG:Ce SCF/ LuAG:Sc SC (1) and LuAG:Pr SCF/LuAG:Sc SC (2) CS, and LuAG:Sc substrate (3) measured in a time range of 3 μs at α particle (a) and □□quanta (b) excitation [27].

For LuAG:Ce SCF/LuAG:Sc SC and LuAG:Pr SCF/ LuAG:Sc SC CS, the differences in decay times at different levels of the luminescence decay (1/e, 0.1, 0.05 and 0.01) under excitation by α-particles and γ-quanta are shown in Fig. 10. The selection of samples with different SCF thicknesses in the 12-30 μm range also enables to analyse the effect of this factor on the separation of decay curves at different types of excitation. The best signal separation from the SCF and SC over the entire time range was achieved in LuAG:Pr SCF/ LuAG:Sc SC structure with a SCF thickness of 12 μm and a 1 mm thick substrate (Fig. 10b). The t_γ/t_α ratios ranges from 9.6 to 15.6 at luminescence intensity decrease from 1/e to 0.05, which is the best result among all the developed types of CS based on LuAG epitaxial structures doped with Ce^{3+}, Pr^{3+} and Sc^{3+} ions.

The LuAG:Ce SCF/LuAG:Sc SC composite scintillator also separates α-particles and γ-quanta (Fig. 10c) with t_γ/t_α in the range of 1.34-1.96 at the scintillation decay from 1/e to 0.01, which is low comparably to that in bare LuAG:Sc substrate (Fig. 4a and Fig. 10c).

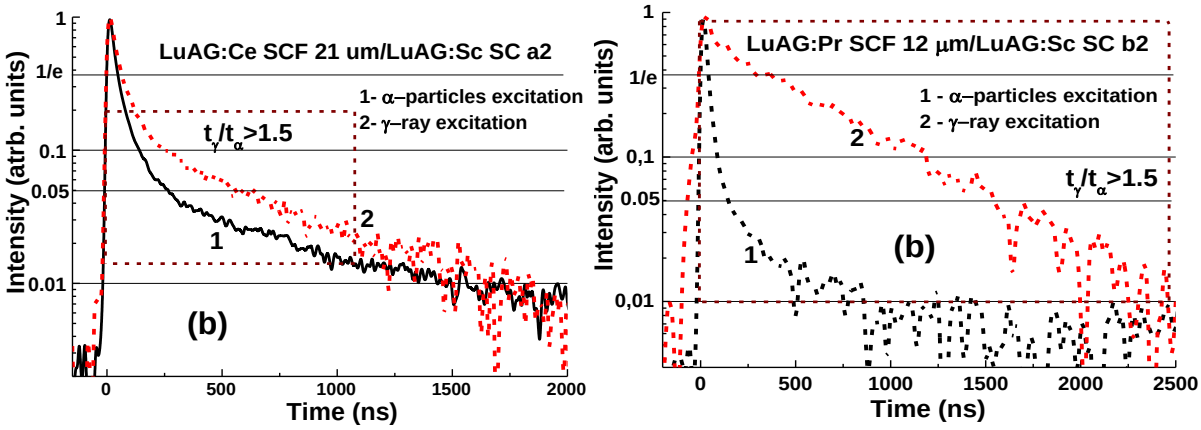

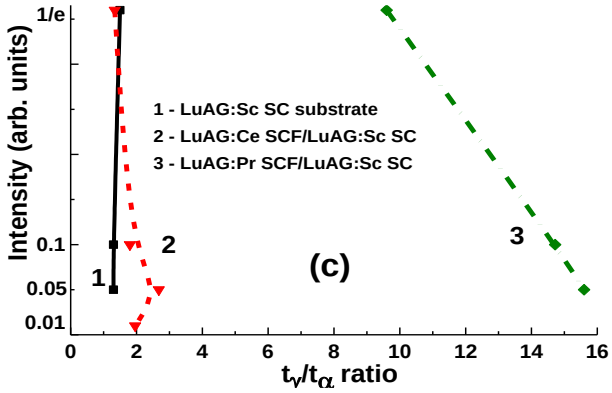

Fig. 10. Scintillation decay of LuAG:Ce SCF/LuAG:Sc SC (a) and LuAG:Pr SCF/ LuAG:Sc SC (b) CS under excitation with α-particles (1) and γ quanta; (c) - t_γ/t_α ratio for different levels of scintillation decay of LuAG:Ce SCF/LuAG:Sc SC (2) and LuAG:Pr SCF/LuAG:Sc SC (3) CS compared to that in LuAG:Sc substrate (1) [18].

3.2. CS based on $Gd_3Al_{2.5}Ga_{2.5}O_{12}$:Ce substrates

3.2.1. Characterization of GAGG:Ce substrates

Successful crystallization of SCFs and bulk ingots of mixed garnets $(Lu, Gd, Tb)_3(Al,Ga)_5O_{12}$:Ce opens new avenues in the engineering of new types of film-substrate CS. Firstly, lower density and Z_{eff} of mixed garnet SCF yields a lower ability to absorb γ-quanta compared to LuAG that should provide better signal separation under mixed radiation fluxes. Secondly, $Gd_3Al_{5-x}Ga_xO_{12}$ (x=2-3) garnets are characterized by a very high LY under γ quanta (^{137}Cs, 662 keV) up to 50 000 photon/MeV [42] compared to LuAG:Ce, LuAG:Pr and LuAG:Sc substrates. For these reasons, SCFs and SC of mixed garnets are a good choice for enhanced CS.

There were two types of the available $Gd_3Al_{5-x}Ga_xO_{12}$:Ce substrates with x = 2.5 and 3 and a thickness of 1 mm. The scintillation decay curves of these substrates under excitation by □□particles and □□quanta are presented in Fig. 11. It was observed that the scintillation decay of substrates under γ-quanta excitation is systematically faster than that under α-particles, which is caused by a specific interaction of these radiations with the scintillator material. The difference in light yield of the GAGG:Ce substrates at these excitation types expressed by the LY_α/LY_γ ratio is in the range of 0.195-0.2 [20, 22].

As one may see in Fig. 11a, an increase in the Ga concentration from x = 2.5 to 3 leads to a significant acceleration of scintillation decay for both excitation types, as well as better separation of the scintillation decay under □□ particles and □-quanta with the t_γ/t_α ratio of 1.46-1.49 at scintillation decay from 1/e to 0.01 as compared to 1.17-1.26 for GAGG:Ce with x = 2.5 (Fig. 11b).

Table 2. Real compositions of $Gd_3Al_{5-x}Ga_xO_{12}$:Ce SCF, type of substrate, h - SCF thickness, T_g- SCF growth temperature, f_g - SCF growth rate, LY – light yield under α-particle excitation from ^{239}Pu and ^{241}Am sources with respect to the standard YAG:Ce SCF sample with a LY of 2.65 photons/KeV [20, 22].

No SCF and SC	Nominal SCF content in melt-solution	Substrate type	Real SCF compositions	h, μm	T_g, °C	f_g, μm/min	LY, % Pu^{239} (12 □s)	LY, % Am^{241} (3 □s)
YAG:Ce	$Y_3Al_5O_{12}$:Ce	YAG	$Y_3Al_5O_{12}$:Ce	54			100	
GAGG2.5:Ce	$Gd_3Al_{2.5}Ga_{2.5}O_{12}$:Ce	-	-	900			340	100
GAGG3:Ce	$Gd_3Al_2Ga_3O_{12}$:Ce	-	-	900			320	
GAGG2:Ce	$Gd_3Al_3Ga_2O_{12}$:Ce	GAGG2.5:Ce	$Gd_{3.038}Ce_{0.005}Pb_{0.001}Al_{3.792}Ga_{1.162}O_{12}$	34	970	1.13	59	18.4
GAGG3:Ce	$Gd_3Al_2Ga_3O_{12}$:Ce	GAGG2.5:Ce	$Gd_{3.08}Ce_{0.003}Pb_{0.077}Al_{3.141}Ga_{1.67}O_{12}$	51	1000	1.15	42	27.1
GAGG3.5:Ce	$Gd_3Al_{1.5}Ga_{3.5}O_{12}$:Ce	GAGG2.5:Ce	$Gd_{3.28}Ce_{0.009}Pb_{0.056}Al_{2.528}Ga_{2.17}O_{12}$	45	974	0.56	32	29.9
GAGG4:Ce	$Gd_3AlGa_4O_{12}$:Ce	GAGG2.5:Ce	$Gd_{3.29}Ce_{0.017}Pb_{0.012}Al_{2.615}Ga_{2.615}O_{12}$	36	985	1.2	31	17.9

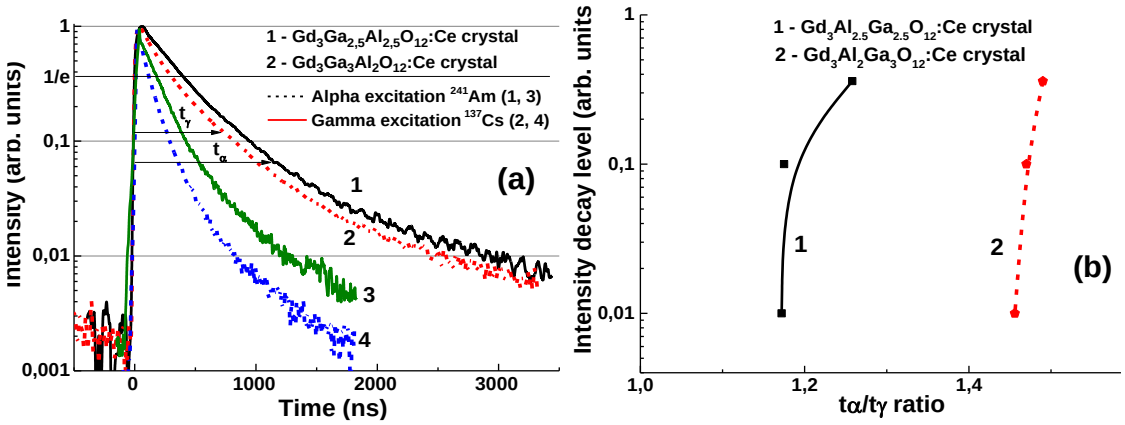

Fig. 11. Scintillation decay curves of GAGG2.5:Ce and GAGG3:Ce crystals under α-particle excitation (curve 1) and □-ray excitation (curve 2). (b) t□/t□ ratio of scintillation decay to 1/e, 0.1, 0.05, 0.01 levels for GAGG2.5:Ce (1) and GAGG3:Ce 3.0 (2) crystals [20, 22].

3.*2.2. CS based on the GAGG:Ce crystals and SCF*

The results of previous research of the scintillation properties of $Gd_3Al_{5-x}Ga_xO_{12}$:Ce (GAGGx:Ce) SCs and SCFs [64, 65] open wide possibilities for development of the *new types of CS based on the mixed garnets with different* Ga^{3+} *concentration*. Scintillation decay kinetics of SCF and single crystals parts of CS based on the mentioned mixed garnets can be specially optimized and fitted due to different Ga content [16, 20, 22]. This will lead to better separation of scintillation signals for the detection of different types of ionizing radiation.

Strong modification of the scintillation decay kinetics of SCF doped with Ce^{3+} LuAG and mixed grenades is observed due to co-doping with M^{2+} (M= Mg^{2+}, Ca^{2+}) and formation of partial cerium ions in the Ce^{4+} charge state [70-74]. In this way, the scintillation decay kinetics of the doubly doped garnet compounds of Ce^{4+} -M^{2+} garnet are strongly accelerated. However, the LY of these SCF scintillators is significantly reduced due to the lower scintillation efficiency of Ce^{4+}-M^{2+} centers compared to the "conventional" Ce^{3+} center. In our opinion, however, such an approach may also be interesting in the case of creating CS based on simple or mixed compounds of garnets with a relatively similar cation content.

In this part of the report we present the results of the development of new types of CS based on SC and SCF of Ce^{3+} doped GAGGx: Ce garnet with different Ga x concentration by LPE growth method [22].

The real compositions of GAGG:Ce SCs and SCF (Fig. 12) are presented in Table 2. According to these results, the Ga ions segregation coefficient in SCF $Gd_3Al_{5-x}Ga_xO_{12}$:Ce SCFs grown on GAGG2.5:Ce SC melt solution at x=2-4 *is equal to 0.58-0.65*. For this reason, the real x concentration of Ga in the SCF samples GAGG2:Ce, GAGG3:Ce, GAGG3.5:Ce and GAGG4:Ce SCF samples is 1.16; 1.67; 2.17 and 2.615, respectively.

Overall, the LY in $Gd_3Al_{5-x}Ga_xO_{12}$:Ce (x=2-4) SCF decreases with Ga content (Table 2). Namely, with excitation of the α-particle by the ^{239}Pu source (5.15 MeV), it is 2-3 times lower than in the reference YAG: Ce SCF sample and more than 5-10 times lower compared to the GAGG:Ce substrate. This phenomenon is caused by a higher concentration of Pb^{2+} flux and lower Ce^{3+}/Pb^{2+} ratios in Gd-rich SCF samples compared to YAG:Ce SCF due to the increase of the lattice constant, namely the volume of dodecahedron localization sites relatively large Pb^{2+} ions [22, 23] .

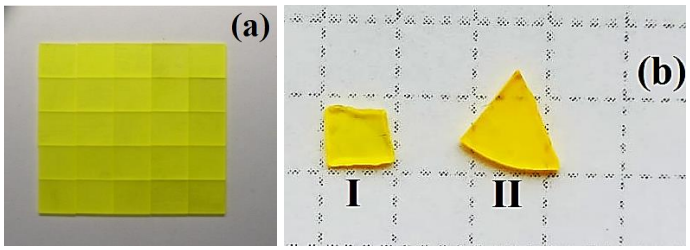

Fig. 12. Substrates prepared from GAGG2.5:Ce crystal (a) and two CS based on $Gd_3Al_3Ga_2O_{12}$:Ce SCF (GAGG2:Ce) (bI) and $Gd_3Al_2Ga_3O_{12}$:Ce (GAGG3:Ce) (bII) SCFs grown onto GAGG2.5:Ce substrates [22].

It is well known that the Pb^{2+} ion is a very effective quencher of Ce^{3+} luminescence in garnets and other compounds, negatively affecting their scintillation properties [3, 22, 27-29, 64]. The increase in Pb^{2+} contamination and Ce^{3+} concentrations in SCFs GAGG:Ce is stimulated by an increase in the dodecahedral site volume for localization of the relatively large Pb^{2+} ions [22, 59, 60, 62-64]. Indeed, as can be seen in Table 2 and Figure 13, the lead content of $Gd_3Al_{5-x}Ga_xO_{12}$:Ce SCFs is relatively high and increases steadily with Ga content. For this reason, the Ce^{3+}/Pb^{2+} ratio in $Gd_3Al_{5-x}Ga_xO_{12}$:Ce SCFs is 1.4-5, while typical values are 15-17 (Fig. 13) [22, 62-64].

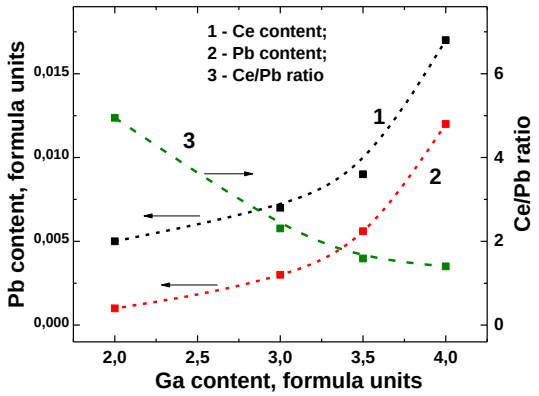

Fig. 13. Dependence of Ce (1) and Pb (2) concentration, as well as Ce/Pb ratio (3) in $Gd_3Al_{5-x}Ga_xO_{12}$:Ce SCFs on nominal Ga content x in melt-solution [22].

The structural quality of $Gd_3Al_{5-x}Ga_xO_{12}$:Ce SCFs with different Ga concentrations was studied, as well as the lattice constant a of SCF samples and the misfit between the lattice constants of SCFs and GAGG:Ce substrate $\Delta a = (a_{SCF} - a_{sub}) / a_{sub} * 100$ % (Fig. 14). The lattice constant of Gd_3Al_{5-x} Ga_xO_{12}:Ce SCFs in the 12.168 -12.235 Å range and *m* value in the -0.51 % < m< + 0.06 % range depend linearly on the Ga x content in these samples. It should be noted that such small mismatch values are very suitable for the deposition of SCF scintillators with high structural and optical quality.

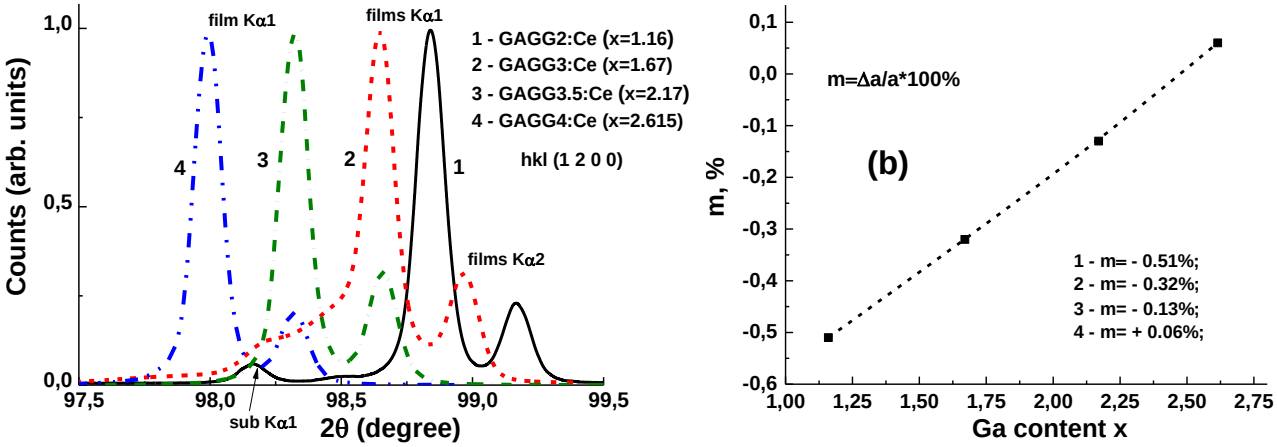

Fig. 14. (a) - XRD of $Gd_3Al_{5-x}Ga_xO_{12}$:Ce SCFs grown from melt solution with the nominal Ga content x in the 2-4 range and real Ga content in the x=1.16-2.615 range; (b) – dependence of misfit *m* on Ga content x in SCF samples [22].

The absorption spectra of CS $Gd_3Al_{5-x}Ga_xO_{12}$:Ce/GAGG2.5:Ce (x=1.16-2.615) compared to the spectra of the GAGG2.5:Ce substrate are shown in Fig. 15. It is worth noting that the absorption spectra of composite structures are a superposition of the spectra of the GAGG:Ce substrate and two SCF samples on either side of these substrates. The sharp bands peaked at 275 and 313 nm in the substrate spectrum and all SCFs attributed to the absorption band of Gd^{3+} ions strongly overlap with the absorption bands peaked in the 260-265 nm range caused by the intrinsic $^1S_0 \rightarrow {}^3P_1$ transitions in Pb^{2+} [22, 62, 63].

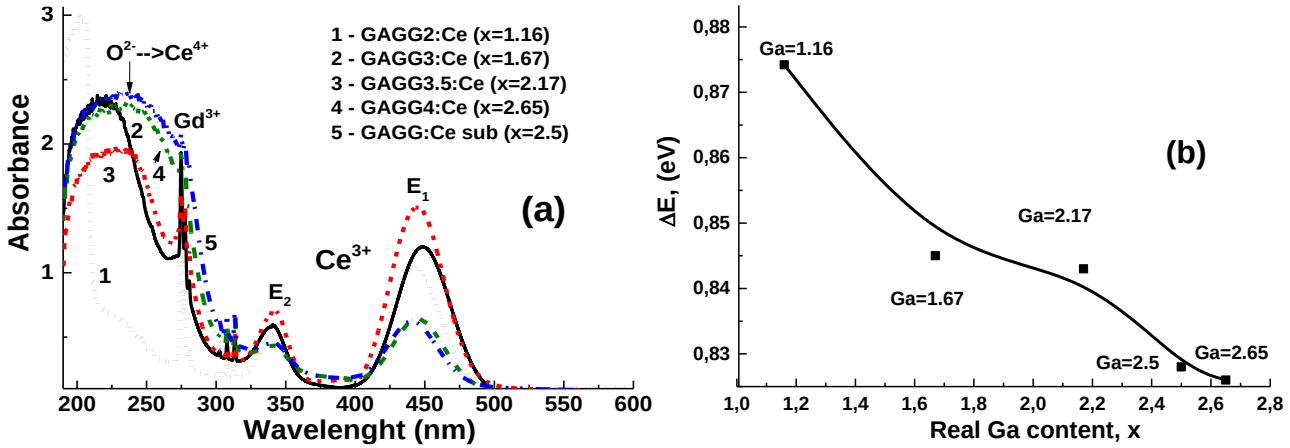

Fig. 15. Absorption spectra (a) of $Gd_3Al_{5-x}Ga_xO_{12}$:Ce (x=2-4) SCFs, grown onto GAGG2.5:Ce substrates (2-5) in comparison with GAGG:Ce 2.5 substrate absorption spectra (curve 1) [22] .

The wide absorption bands of CS $Gd_3Al_{5-x}Ga_xO_{12}$:Ce/GAGG2.5:Ce with different Ga concentration in SCF samples and GAGG2.5:Ce substrate in the range of 339-341 nm and 440-450 nm (marked as E2 and E1 bands, respectively) are associated with the 4f-5d (^{2}E) transitions of Ce^{3+} ions. The remaining Ce^{3+} absorption bands in these scintillators are below 230 nm and are related with the 4f-5d (T_{2g}) transitions [62, 63]. As the Ga content increased in the range of 1.16-2.65 in $Gd_3Al_{5-x}Ga_xO_{12}$:Ce SCF, we observed a shift of the absorption bands E_1 and E_2 in Ce^{3+} (Fig. 15a) and a change in the corresponding values of $\Delta E = E_2 - E_1$ (Fig. 15b). The value of □E is the largest in the composite scintillator sample with the smallest Ga content in SCF (x=1.16) and it systematically decreases with increasing Ga concentration in SCF, because Ga concentration approaches the gallium concentration x = 2.5 in GAGG substrate: Ce (Table 2).

The absorption spectra of CS $Gd_3Al_{5-x}Ga_xO_{12}$:Ce/GAGG2.5:Ce (x=1.16-2.615) show the presence of an additional broadband peak at about 255 nm (Fig. 15). Most probably, this band is related to the $O^{2+} \rightarrow Ce^{4+}$ charge transfer transitions (CTT) (see [70-74] for details). The formation of Ce^{4+} states in these SCFs, especially in the samples with the highest Ga content, is due to the inclusion of the impurity associated with the

Pb^{2+} flux (Table 2). Indeed, the intensity of $O^{2+} \rightarrow Ce^{4+}$ CTT band peaked at 255 nm systematically increases in the absorption spectra of $Gd_3Al_{5-x}Ga_xO_{12}$:Ce SCF / GAGG2.5:Ce CS as Ga content x rises from 1.16 to 2.615 in SCF (Fig. 15). Such phenomenon correlates well with remarkable increase in Pb concentration in Ga-rich SCF samples (see Table 2).

The content of large Pb^{2+} ions in SCF samples with the largest Ga concentration may be contributed to the decrease in their LY (see Table 2). A negative influence of Pb^{2+} on the LY of epitaxially grown films was observed in many scintillators [3, 22, 27-29, 62-64]. Such influence can be attributed to the creation of Pb^{2+}-Ce^{4+} pairs due to charge and volume compensation at relatively large concentration of lead ions in SCF samples and subsequent reduction in Ce^{3+} concertation ions in garnet hosts (see [70-73] for details).

Normalized CL spectra of the SCF part $Gd_3Al_{5-x}Ga_xO_{12}$:Ce SCF of CS with the range x = 1.16-2.16 and the substrate GAGG2.5:Ce is shown in Fig. 16. The CL spectra of all SCF and the substrate show only the wide luminescence of the Ce^{3+} ion band in the visible range, they peaked at 545-551 nm assigned to the $5d^1 \rightarrow 4f$ ($^2F_{5/2;7/2}$) transitions of the Ce^{3+} ion in the mentioned garnet hosts. Ce^{3+} luminescence peaks in $Gd_3Al_{5-x}Ga_xO_{12}$:Ce SCFs are clearly shifted in the blue direction, and the FWHM of these bands increases with increasing Ga content in SCF in the range x = 1.16-2.16. These trends are well consistent with the results of similar studies of the CL $Gd_3Al_{5-x}Ga_xO_{12}$:Ce SCFs spectra disclosed in [62-64] and can be explained by the decreasing crystal field strength at the dodecahedral position of the respective garnet hosts. An exception is the CL spectrum of the GAGG2.5:Ce substrate, which shows a lower FWHM than the corresponding SCF (Fig. 16, curve 5). However, this effect is due to the strong reabsorption of the high-energy wing of the emission band with the corresponding absorption band 4f-5d of Ce^{3+} ions with a peak of 442 nm in a thick crystalline substrate compared to that in thin SCF with similar compositions

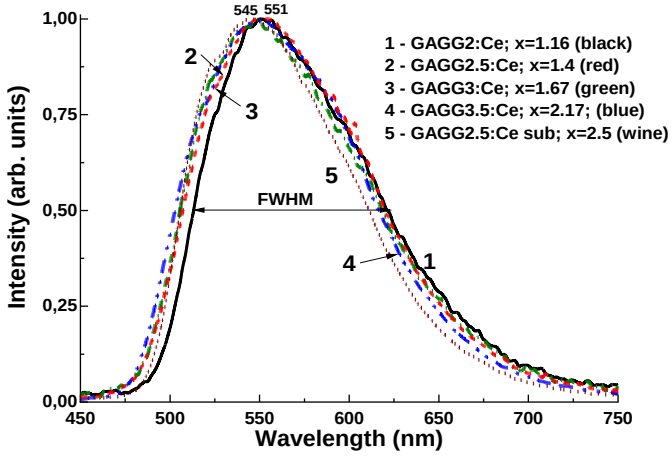

Fig. 16. Normalized CL spectra of $Gd_3Al_{5-x}Ga_xO_{12}$:Ce (x=1.16-2.17) SCF in comparison GAGG2.5:Ce substrate (5) [29].

The PHS registered with $Gd_3Al_{5-x}Ga_xO_{12}$:Ce SCF/GAGG2.5:Ce CS with Ga concertation in the SCF in the x=1.16-2.65 range under excitation by α-particles and γ- rays of ^{137}Cs source are presented in Figs. 18a

and 18b, respectively. The main peaks in Fig. 18a correspond to the total absorption of α-particles, while the peaks in the left part of the spectra are related to the absorption of the low-energy emission from ^{241}Am source.

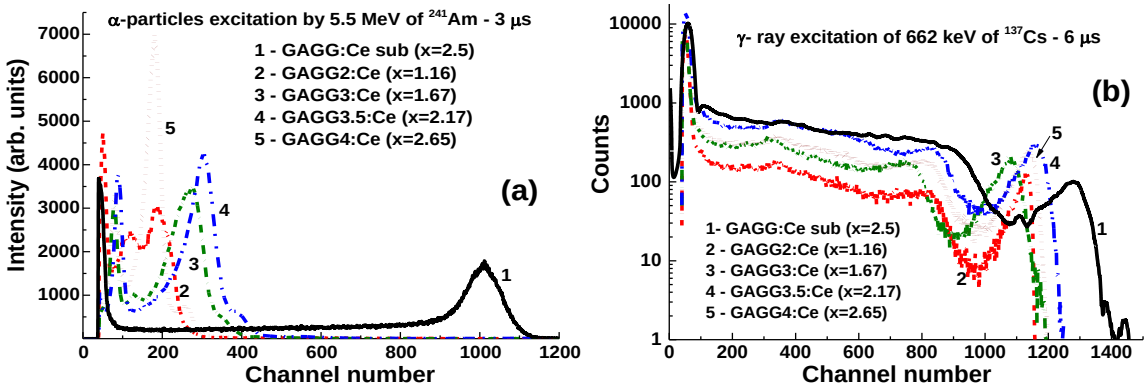

Fig. 17. PHS of $Gd_3Al_{5-x}Ga_xO_{12}$:Ce SCF/GAGG:Ce SC CS (2-5) with the different Ga content x = 1.6-2.67 in SCF (2-5) and GAGG:Ce substrate (1) measured under α-particle excitation with energies of 59.6 keV and 5.5 MeV of ^{241}Am source (a) and γ-excitation with an energy of 662 keV of ^{137}Cs source (b) [22].

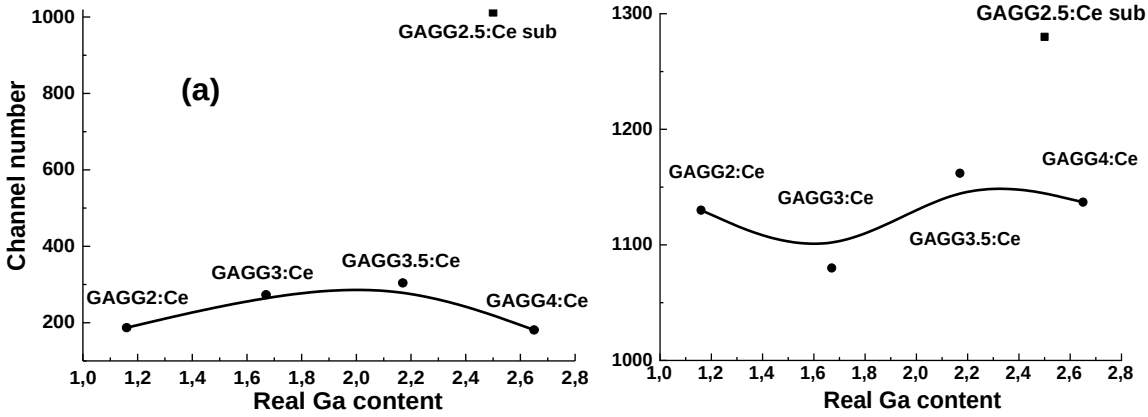

Fig. 18. Location of the main photopeak of $Gd_3Al_{5-x}Ga_xO_{12}$:Ce SCF/GAGG2.5:Ce SC CS and GAGG2.5:Ce substrate under excitation by α-particles (a) and γ quanta (b) [22].

It should be noted that the positions of the main photopics of the source of the ^{241}Am α-particles observed in Fig. 18a and 19a are significantly different for all $Gd_3Al_{5-x}Ga_xO_{12}$:Ce SCF/GAGG:Ce CS and the GAGG2.5:Ce substrate. This means that *the α-particles excite only parts of the SCF of the CS*. The largest scintillation efficiency was registered with composite scintillator with a Ga content of x=2.17 in the SCF part; however, the LY of this sample is by more than 3 times lower than that of GAGG:Ce substrate (Figs. 17a and 18a).

Under γ-excitation of $Gd_3Al_{5-x}Ga_xO_{12}$:Ce SCFs/GAGG:Ce CS the main peaks in the pulse high spectra correspond to the total absorption of 662 keV γ-rays (Fig. 17b). The additional peak at 32 keV relates to the low-energy line of ^{137}Cs source.

Quite similar positions of the main peaks are observed in Figs. 17b and 18b for all CS and GAGG2.5:Ce substrate, becuase γ-rays excite mainly the substrates in $Gd_3Al_{5-x}Ga_xO_{12}$:Ce SCFs / GAGG2.5:Ce epitaxial structures, and contribution of SCF scintillators to the total LY of CS is insignificant.

The difference in the scintillation decay curves of the bulk and film components of CS is determined by the analysis of decay curves in a broad decay intensity range under α–particle and γ-ray excitation of GAGG:Ce substrates with different Ga content. We performed such an analysis for the GAGG2.5:Ce substrate and the GAGG3:Ce reference crystal with the same thickness of 0.9 mm for scintillation decay to levels 1/e, 0.1, 0.05 and 0.01 with excitation with α-particle ^{239}Pu (5.5 MeV) and γ-ray ^{167}Cs (662 KeV) radiation sources (Table 2). The deconvolution of the corresponding decay curves was performed using the approximation $I = A_i \exp(-t/\tau_i) + const$, and its results are presented in Table 2. To quantify the differences in decay curves at the 1/e, 0.1, 0.05, 0.01 levels, the t_α/t_γ ratios for respective decay times were used (Table 3 and Figs. 19 and 20).As shown in Fig. 19a,b, both GAGG2.5:Ce and GAGG3:Ce crystal decay curves under the γ-quantum excitation are systematically faster than in the case of excitation with α–particle. It is the fundamental behavior of scintillation materials related to the specific interaction of α-particles and γ-quanta with the scintillator material with different cation content. This effect is quantified by the t_α/t_γ ratios in GAGG2.5:Ce substrate and reference GAGG3:Ce crystal (Fig. 20). As can be seen in this figure, the ratio t_α/t_γ varies in the range 1.17-1.26 and 1.46-1.49 respectively, *and the value of this ratio is much higher in garnet crystals with high Ga content*. Meanwhile, taking into account the slower decay and smaller differences in the t_α/t_γ ratio in GAGG2.5:Ce crystals, such compositions are more suitable in the development of CS based on the decay curves differences of GAGG:Ce-based substrate and $Gd_3Al_{5-x}Ga_xO_{12}$:Ce SCFs (x=1.16-2.615) (Fig. 19).

The separation rate of the scintillation signal at the registration of α-particles and γ-rays may be improved in the epitaxial structures based on the SCFs and SCs of $Gd_3Al_{5-x}Ga_xO_{12}$:Ce garnets with the different Ga content. Indeed, Fig. 19 substantial differences in the scintillation decay are observed in the four types of $Gd_3Al_{5-x}Ga_xO_{12}$:Ce SCF/GAGG2.5:Ce CS at x=1.16 (a); 1.67 (b); 2.17 (c) and 2.65 (d) under α-particles and γ-quanta. Fig. 20 demonsstrates the t_α/t_γ ratios for scintillation decay to the 1/e, 0.1, 0.05 and 0.01 levels for these CS types (curves 1-4), respectively.

Decay time values to the mentioned levels for four samples of CS under α-particle and γ-quanta excitations are presented in Table 3. Note here that the decay profiles of $Gd_3Al_{5-x}Ga_xO_{12}$:Ce SCF scintillators under □□ particle excitation *shows weak correlation with Ga content in the 1.16-2.165 range*. Therefore, the observed significant differences in scintillation decay of $Gd_3Al_{5-x}Ga_xO_{12}$:Ce SCFs under α-particle excitation (Fig. 19) in comparison with bulk crystals (Fig. 11) are *mainly due the Pb^{2+} doping and recharging the part of Ce^{3+} ions to Ce^{4+} state in SCF*

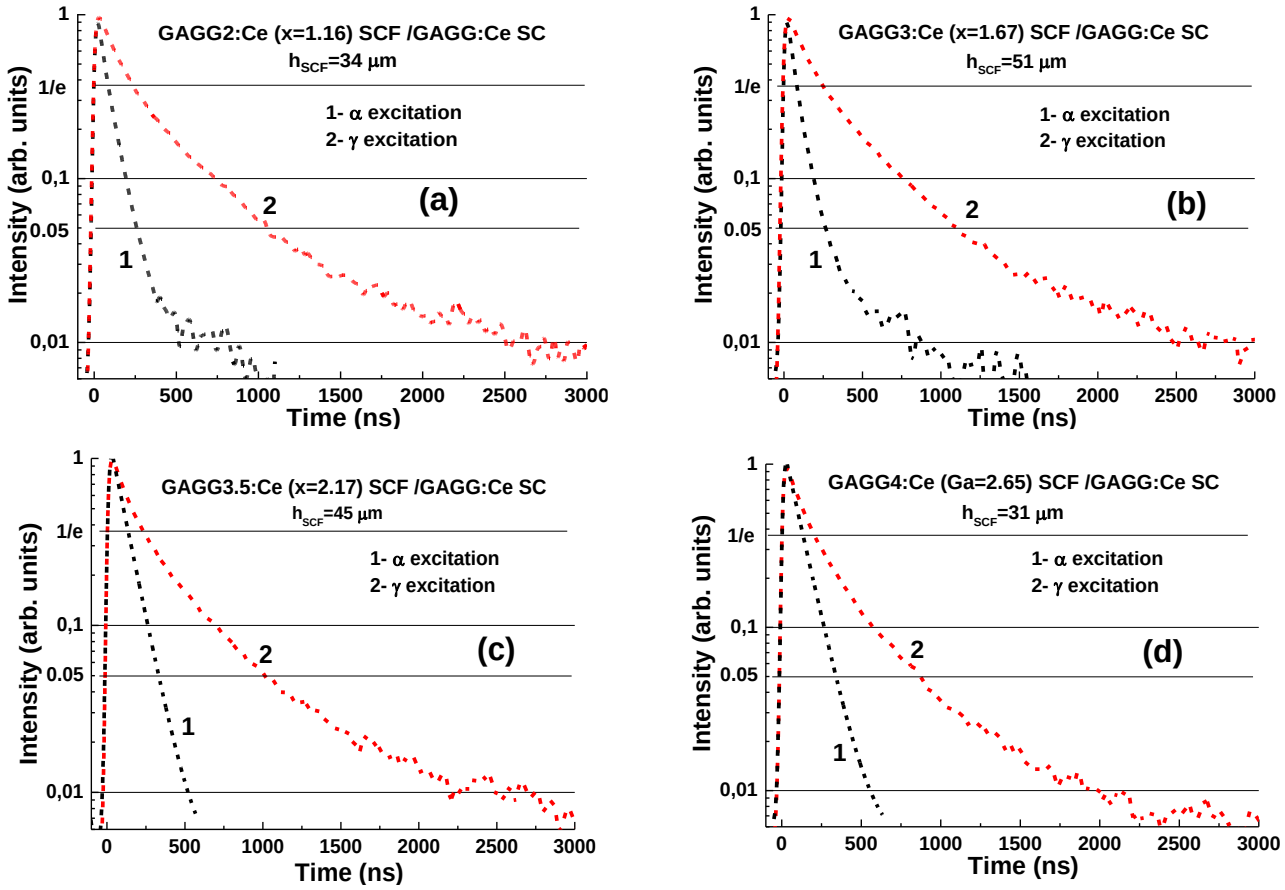

Fig. 19. Scintillation decay curves of $Gd_3Al_{5-x}Ga_xO_{12}$:Ce SCF/GAGG2.5:Ce CS containing SCF with Ga content x = 1.16 (a); 1.67 (b); 2.17 (c) and 2.65 (d) grown onto GAGG:Ce 2.5 substrates under α-particle excitation (curves 1) and □-ray excitation (curves 2) [29].

Table 3. $t_{□}$ and $t_{□□}$values of scintillation decay to 1/e, 0.1, 0.05, 0.01 intensities of $Gd_3Al_{5-x}Ga_xO_{12}$:Ce SCF/GAGG2.5:Ce SC CS with varied Ga concentrations in SCF under α-particle and □-ray excitation.

	GAGG2.5:Ce substrate		**GAGG2:Ce SCF/ GAGG:Ce sub**		**GAGG3:Ce SCF /GAGG:Ce sub**		**GAGG3.5:Ce SCF /GAGG:Ce**		**GAGG4:Ce SCF /GAGG:Ce sub**	
	$t_{□□□}$ns	$t_{□□□}$ns	$t_{□□□}$ns	$t_{□□□}$ns	$t_{□□□}$ns	$t_{□□□}$ns	$t_{□□□}$ns	$t_{□□□}$ns	$t_{□□□}$ns	$t_{□□□}$ns
1/e	390	310	87	2239	86	252	129	235	133	208
0.1	925	790	207	742	205	776	270	700	275	583
0.05	1300	1170	280	1072	287	1128	345	1029	355	888
0.01	2875	2465	638	2540	835	2554	533	2254	590	1976

scintillators [22, 62-64]. This causes the scintillation decay acceleration in doubly doped Ce^{4+}-Pb^{2+} SCF scintillators. Furthermore, such phenomenon *enables the separation of the decay kinetics of SCF scintillators even in the case of similar Ga content in the x=2.17-2.615 range (Fig.19, c and d) with Ga concentration x=2.5 in*

the substrate. These results are well consistent with the previously published data on the scintillation properties of SCFs and SCs of $Gd_3Al_{5-x}Ga_xO_{12}$:Ce garnets [22].

An efficient separation of the signals from SCF and SC substrate at 1/e, 0.1 and 0.05 intensities (Figs. 19 and 20) can be obtained *for all the developed types of CS in the whole 100-3000 ns time range*. Furthermore, the largest differences in the scintillation decay curves of CS under α- and γ- excitations were observed between the 0.1 and 0.01 levels. The best α/γ separation is observed with $Gd_3Al_{5-x}Ga_xO_{12}$:Ce/GAGG2.5:Ce epitaxial structures at x=1.16 and 1.67 (Fig. 20, curves 2 and 3). The t_γ/t_α ratio was in the 2.75-4 range at scintillation decay to 1/e, 0.1 and 0.05 levels. Meanwhile, *taking into account the high LY of SCF scintillator and a high t_γ/t_α ratio for SCF and SC parts of CS equal to 1.8-4.2 at 1/e, 0.1 and 0.05 levels of the intensity decay (Fig. 20, curve 4), the best scintillation figure-of-merit is observed for $Gd_3Al_{2.83}Ga_{2.17}O_{12}$:Ce:Ce SCF/GAGG2.5:Ce epitaxial structure*.

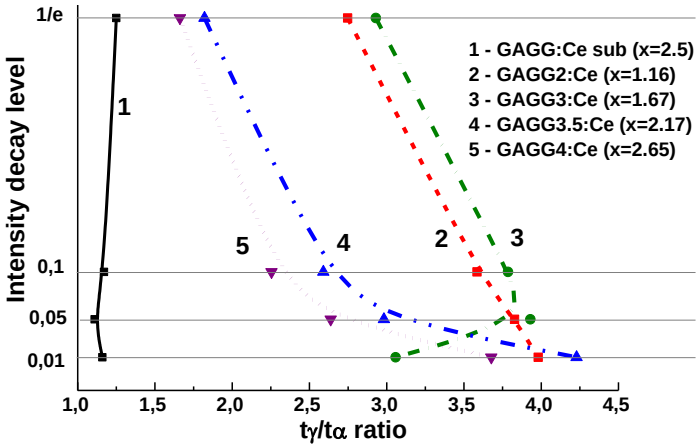

Fig. 20. Plot of t_γ/t_α ratio on scintillation decay to 1/e, 0.1, 0.05, 0.01 levels for GAGG2.5:Ce substrate (1) and $Gd_3Al_{5-x}Ga_xO_{12}$:Ce SCF/GAGG2.5:Ce CS with different Ga contents x (2-5) [22].

3.2.3. Scintillating screens based on the LPE-grown Ce^{3+}-doped $Tb_3Al_5O_{12}$ and $Tb_{3-x}Gd_xAl_{5-y}Ga_yO_{12}$ garnets

Cation composition engineering opens new possibilities in the development of scintillators based on SCFs of mixed garnets. Crystallization of SCFs on different substrates using different fluxes enables optimization of excitation transfer deficiency to activators to ensure a high scintillation efficiency of CS. The band gap and position of 5d energy levels of Ce^{3+} ion in the bandgap may be controlled by a combination of Gd^{3+}, Tb^{3+} and Ga^{3+} cations (see Fig. 2). These corresponding changes in crystal field strength are caused by of Gd^{3+} and Tb^{3+} cation substitution in dodecahedral positions and Ga^{3+} ions by Al^{3+} cations both in the tetrahedral and octahedral positions in the garnet lattice.

Following the successful tests of GAGG:Ce SCF/GAGG:Ce SC CS, SCFs of LuAGG:Ce and TbAG:Ce were crystallized (Fig. 21) [20, 21] by LPE method using the $PbO-B_2O_3$ flux both on "traditional" YAG and $Gd_3Ga_{2.5}Al_{2.5}O_{12}$ (GAGG) substrates with the lattice constants of 12.01 and 12.232 Å, respectively, and their structural properties were determined. The measured mismatch of lattice constants for these CS was - 0.73% and

- 1.32%, respectively (Fig. 22), and small enough to obtain SCFs of a good optical quality. Meanwhile, the crystallization of LuAGG:Ce and TbAG:Ce SCFs on GAGG:Ce substrates with x=3.0 failed due to a large mismatch over 2%. According to XRD measurements, the lattice constant mismatch (m) between TbAG:Ce SCF and YAG and GAGG substrates was + 0.53-0.56% and - 1.29%, respectively (Table 4). TbAG SCF crystallization on YAG and GAGG substrates with such large mismatch is complicated due to the formation of a transitional zone in the form of a solid solution at the film-substrate interface reducing this mismatch.

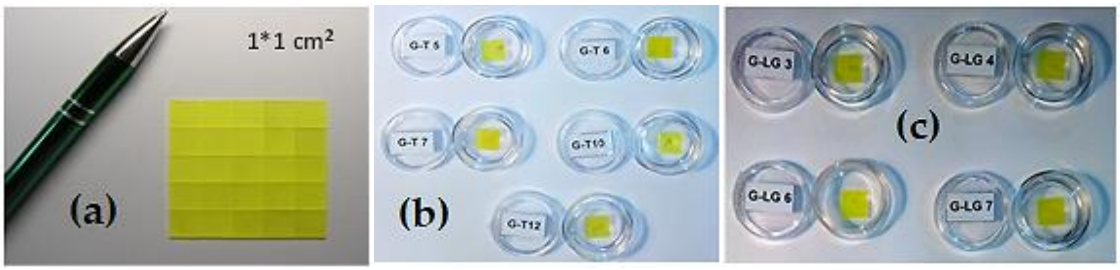

Fig. 21. GAGG:Ce substrates (a); TbAG:Ce SCF/GAGG:Ce SC (b) and LuAG:Ce SCF/GAGG:Ce SC (c) CS [20, 21].

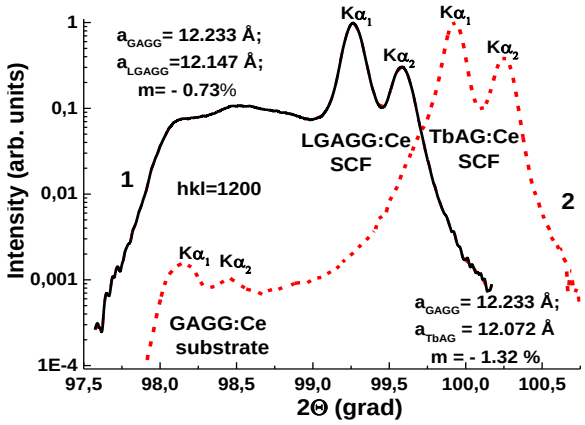

Fig. 22. XRD patterns of LGGAG:Ce SCF/GAGG:Ce SC (1) and TbAG:Ce SCF/GAGG:Ce SC (2) epitaxial structures [20, 21].

Table 4. Misfit between SC and SCF lattice parameters, *m*, CL band maximum, λ_{max}, the ratio of decay times at different levels of scintillation decay, and relative light yield of SCF.

SCF	SC	m, %	□max, nm	$t_{1/e}/t_{1/20}$, ns	LY, %
LuAG:Ce	YAG	-0.82	509	53	205
LuAG:Pr	YAG	-0.8	305	17	79
LuAG:Sc	YAG	-0.8	280	245; 390	96
$Lu_{1.5}Gd_{1.5}Al_5O_{12}$:Ce	YAG	+0.02	548	50	86
$Lu_{1.5}Gd_{1.5}Al_{2.75}Ga_{2.25}O_{12}$:Ce	GAGG	-0.73	519	51/130	145
TbAG:Ce	YAG	+0.55	555	242/1645	253-264

	GAGG	-1.29	560	306/1795	195
$Tb_{1.5}Gd_{1.5}Al_{2.5}Ga_{2.5}O_{12}$:Ce (PbO)	GAGG	-0.12	543	333/990	380
$Tb_{1.5}Gd_{1.5}Al_3Ga_2O_{12}$:Ce (BaO)	GAGG	-1.30	543	228/728	380

TbAG:Ce SCFs crystallized on YAG and GAGG substrates possess 30% higher LY (Table 4) and exceptionally low level of phosphorescence compared to YAG:Ce and LuAG:Ce SCFs. These SCFs are also characterized by relatively fast scintillation decay in the range of 0-1000 ns. Therefore, TbAG:Ce SCFs based on GAGG:Ce substrates are very promising for microtomographic detector screens, as well as a suitable component for CS engineering.

Corresponding changes in crystal field strength caused by substitution of Gd^{3+} by Tb^{3+} in dodecahedral positions and Ga^{3+} by Al^{3+} cations both in the tetrahedral and octahedral positions in the garnet lattice result in the blue- or redshift of the Ce^{3+} luminescence spectrum in $Tb_{3-x}Gd_xAl_{5-y}Ga_yO_{12}$:Ce garnets as Ga^{3+} (Fig. 23a) or Gd^{3+} (Fig. 23b) contents increase. A complex cascade of $Gd^{3+} \rightarrow Tb^{3+} \rightarrow Ce^{3+} \rightarrow Tb^{3+}$ energy transfer is observed in $Tb_{3-x}Gd_xAl_{5-y}Ga_yO_{12}$:Ce with a high concentration of Gd^{3+} and Tb^{3+} cations. The reason of this transfer is the overlap of Gd^{3+} and Tb^{3+} emission bands and Ce^{3+} ion absorption bands in the UV range, as well as Ce^{3+} ion emission bands and Tb^{3+} absorption bands in the blue range.

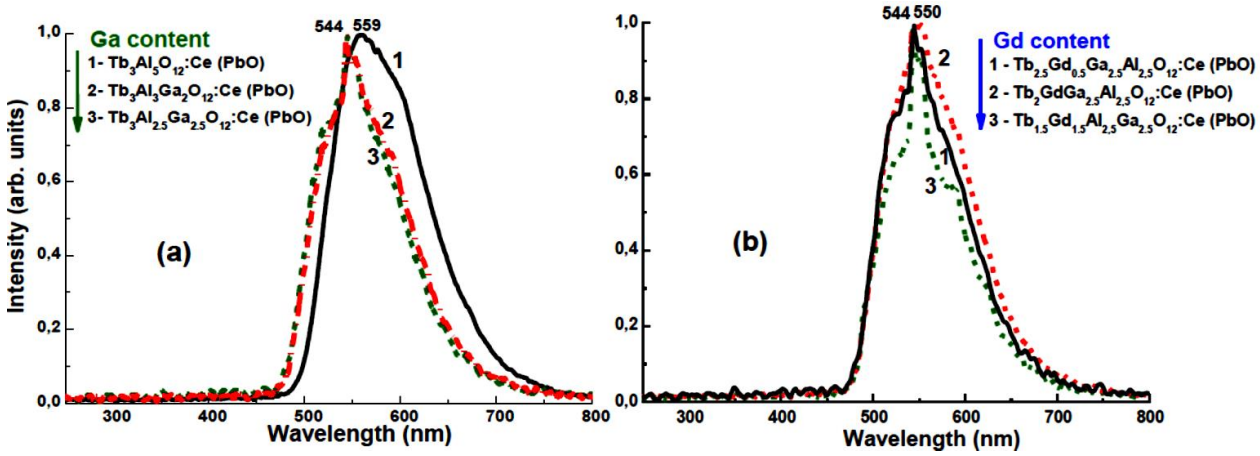

Fig. 23. Normalized CL spectra of $Tb_3Al_{5-y}Ga_yO_{12}$Ce (PbO) (a), $Tb_{5-x}Gd_xAl_{2.5}Ga_{2.5}O_{12}$:Ce (PbO) (b) SCFs with different x and y (see figure legend) [68, 69].

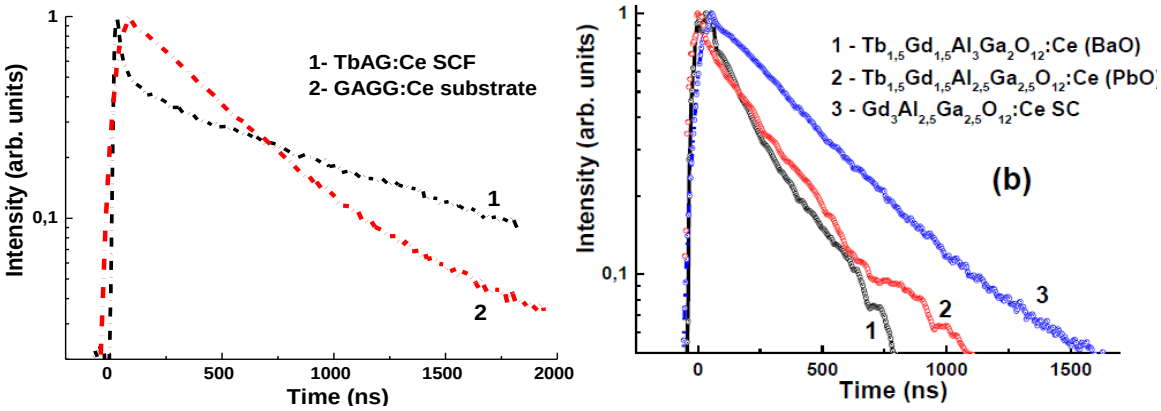

Fig. 24. The normalized scintillation decay of $Tb_3Al_5O_{12}$:Ce SCF (a) $Tb_{1.5}Gd_{1.5}Al_2Ga_3O_{12}$:Ce (BaO) and $Tb_{1.5}Gd_{1.5}Al_{2.5}Ga_{2.5}O_{12}$:Ce in comparison with that in bulk $Gd_3Al_{2.5}Ga_{2.5}O_{12}$:Ce (b, curve 3) [68, 69].

For this reason, optimization of Gd^{3+}, Tb^{3+}, Ga^{3+} contents in $Tb_{3-x}Gd_xAl_{5-y}Ga_yO_{12}$:Ce garnet at x=1.5 and y=2-2.5 provides a significant improvement in the film scintillation efficiency due to more favorable excitation energy transfer conditions caused by changes in the band gap and Ce^{3+} energy structure.

$Tb_{3-x}Gd_xAl_{5-y}Ga_yO_{12}$:Ce (PbO) SCFs demonstrate a very high structural quality, while the SCFs grown from the BaO flux possess excellent scintillation properties, but the structure quality is slightly lower due to the high flux density. It is very important that the scintillation decay kinetics of the $Tb_{1.5}Gd_{1.5}Al_{2.5}Ga_{2.5}O_{12}$:Ce (PbO) and, especially, $Tb_{1.5}Gd_{1.5}Al_3Ga_2O_{12}$:Ce (BaO) SCFs is notably faster by at least 2 times in the range of 0-2 μs as compared to GAGG:Ce crystal (Fig. 25). These SCFs and high-quality $Gd_3Al_{2.5}Ga_{2.5}O_{12}$:Ce crystals can be used in CS for simultaneous registration of different components of ionization fluxes.

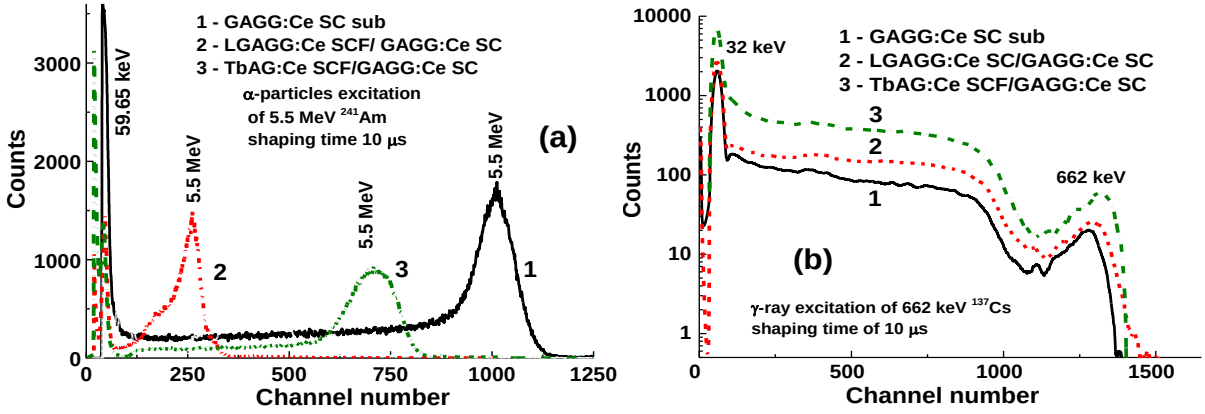

Fig. 25. PHS of LGAGG:Ce SCF/ GAGG:Ce SC (2), TbAG:Ce SCF/GAGG:Ce SC (3), and GAGG:Ce substrate (1) measured in a time range of 10 μs at excitation with α-particles (a) and □□quanta (b) [20, 21].

The results obtained on CS based on LuAG:Pr and LuAG:Sc substrates indicate that the simultaneous excitation of the substrate and film by γ-quanta significantly affects their pulse height spectra (Fig. 7b and 9b) and scintillation decay kinetics (Fig. 8 and 10). In contrast, in LGAGG:Ce SCF/GAGG:Ce SC and TbAG:Ce SCF/GAGG:Ce CS, □□particles excite only SCFs, which is indicated by the different locations of the main peaks in the PHS spectra (Fig. 25a). Under excitation by □□quanta, the main peaks of both CS and GAGG:Ce

substrate almost coincide, which means that the substrate in these composites is mainly excited (Fig. 25b).

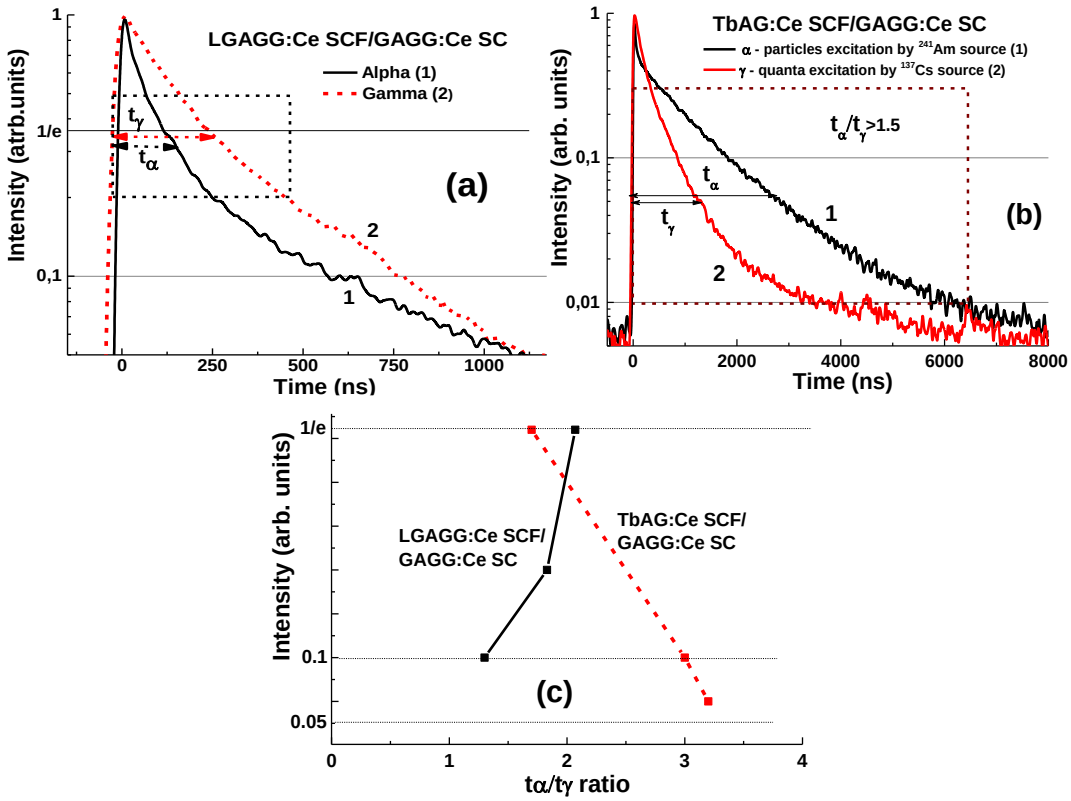

Fig. 26. Scintillation decay of LGAGG:Ce SCF/GAGG:Ce SC (a) and TbAG:Ce SCF/GAGG:Ce SC (b) CS under excitation with α-particles (1) and γ- quanta (2). (c) - t_γ/t_α ratio for different levels of luminescence decay for these two types of composites [20, 21].

A large difference in scintillation decay is observed under □□particle and γ-quanta excitations (Fig. 26a, b) quantified by the tα/tγ ratio, which is 1.3-2.07 and 1.7-3.2 as luminescence decays from 1/e to 0.1 and 0.05 levels, respectively (Fig. 26c). For the LGAGG:Ce SCF/GAGAG:Ce SC composite scintillator, the scintillation signals from the SCF and substrate can also be separated with a high tα/ tγ ratio in a narrow time range of 0 - 500 ns, but in a slightly narrower range of luminescence intensity between 1/e and 0.1 (Fig. 26a). TbAG:Ce SCF/GAGG:Ce SC composite scintillator has superior properties compared to the former epitaxial structure due to the higher tα/tγ in a wide time range of 0 - 6000 ns as luminescence intensity decreases from 1/e to 0.01 (Fig. 26c). These results certify that both these types of CS are capable to discriminate successively α-particles and γ-quanta in mixed ionization beams.

3.3. Composite TL detectors

CS disclosed in the previous sections showed the ability to simultaneous registration of components of mixed ionizing fluxes by their scintillation decay at the excitation with α-particles and-γ quanta. β-particles with energies in a wide range from keV to MeV cannot be detected this way in mixed ionizing beams. The use of CS operating in *in situ* mode is also complicated under registration of low doses of radiation during long-term exposure.

Another option is a registration of thermoluminescence curves (TL) from a SCF and a substrate of a composite material produced by the LPE method. Such TL detectors were based on Ce^{3+}-doped with LuAG and YAG garnets and their capability to detect simultaneously α- and β- particles, and X-ray or γ quanta was verified [23, 24].

3.3.1. LuAG:Ce SCF/YAG:Ce and YAG:Ce SCF/LuAG:Ce SC TL composite materials

The first prototypes of TL composite materials were created based on YAG:Ce SCF/LuAG:Ce SC and LuAG:Ce SCF/ YAG:Ce SC epitaxial structures. The fabrication of such structures by the LPE method was technologically challenging because a misfit in the of SCF and substrate lattice constants, which was about of 0.8% for the both composites (Fig. 27), is less than the border condition value of ±1% for SCF growth of garnet compounds [23].

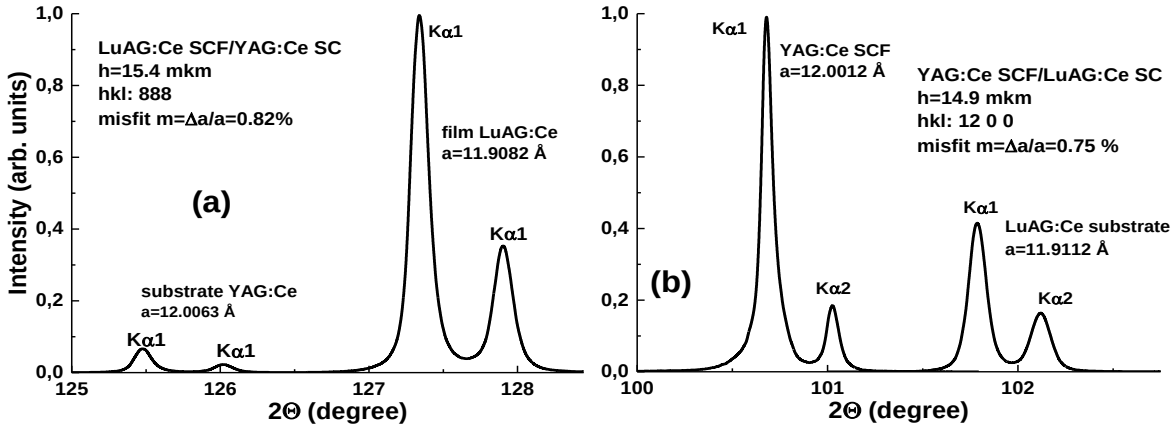

Fig. 27. XRD pattern of epitaxial structures of LuAG:Ce SCF/YAG:Ce SC (a) and YAG:Ce SCF/LuAG:Ce SC (b) [23].

The chosen contents of these composites were based on previous observations of TL properties SCFs and substrates of these garnets, namely a large difference in growth temperature, the gas atmosphere composition, and types of defects and admixtures. Ce^{3+} ions are typically served as hope trapping centers, while TL peaks in Ce^{3+} doped films and crystals of garnet compounds under study correspond to electron trapping centers. Such centers in garnets can be oxygen vacancies and their aggregates with other defects, in particular, substitutional defects related to incorporation of Pb ions in SCF of these materials.

The primary task was to compare the main TL peaks from YAG:Ce and LuAG:Ce SCFs and crystals under excitation by α- and β-particles. α-particles of an ^{241}Am source (5.5 MeV) should be completely absorbed in the SCF part of the composite materials, while β-particles of the ^{90}Sr + ^{90}Y source with an average energy of 1.1 MeV can be absorbed by 1.3 mm thick YAG:Ce and 0.8 mm thick LuAG:Ce substrates. Hence, TL signals from the SCFs and substrates correspond mainly to the registered α-particles and β-particles, respectively.

The main peaks for LuAG:Ce SCF/YAG:Ce SC are registered at temperatures of 325 °C and 215 °C after irradiation with α- and β-particles, respectively (Fig. 28a), while for YAG:Ce SCF/LuAG:Ce CS the corresponding peaks are at 180 °C and 345 °C, respectively (Fig. 28b). Therefore, the difference ΔT between the main TL peaks used as a discrimination measure of these two types of particles is 110 °C and 165 °C for these types of composites, respectively.

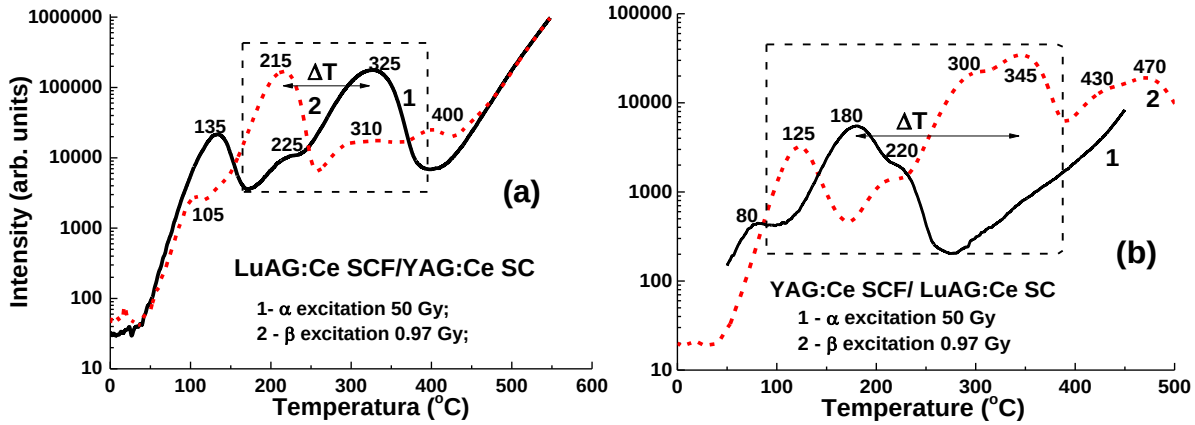

Fig. 28. TL glow curves of LuAG:Ce SCF/YAG:Ce SC (a) and YAG:Ce SCF/LuAG:Ce SC (b) TL composite materials after irradiation with α- (1) and β- (2) particles [23].

3.3.2. $Lu_{3-x}Gd_xAG$:Ce SCF/YAG:Ce SC TL composite materials

Following the successful development of LuAG:Ce/YAG:Ce TL composite materials, LuAG:Ce layers in them were modified by adding Gd. In the $Lu_{3-x}Gd_xAl_5O_{12}$:Ce SCF/YAG:Ce SC structures with x=0-1.5 (Fig. 29), the difference between the main TL peak positions after irradiation with α-and β-particles gradually increases with the increase of Gd content (see [24] for TL details). The obtained difference (ΔT) in the main TL peak locations increased compared to the LuAG:Ce SCF/YAG:Ce SC structures from 110 to 215 °C.

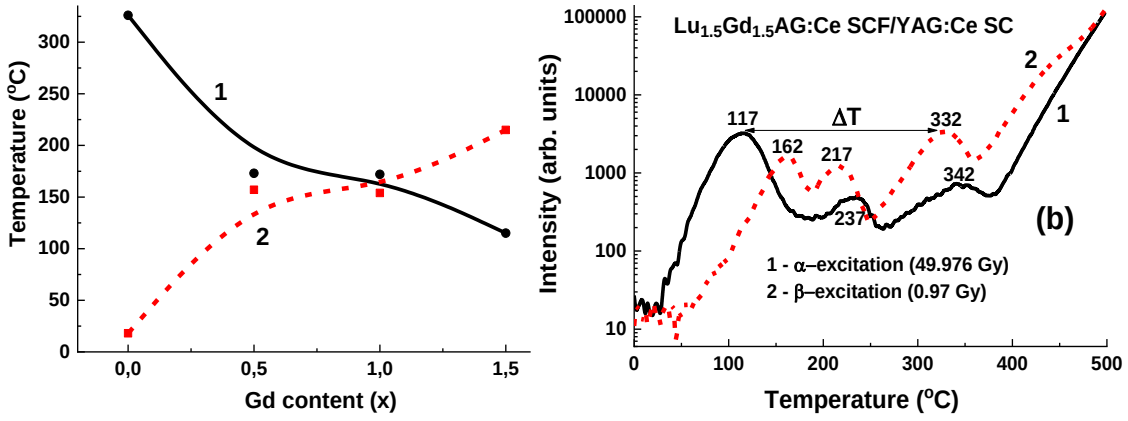

Fig. 29. (a) – Dependence of the main $Lu_{3-x}Gd_xAl_5O_{12}$:Ce SCF/YAG:Ce SC TL peak location on Gd content after excitation with α-particles (1), and the temperature interval between the main TL peaks of the $Lu_{3-x}Gd_xAl_5O_{12}$:Ce SCF film and YAG:Ce substrate after excitation with α (^{241}Am) and β (^{90}Sr + ^{90}Y) particles (2). (b) – glow curves of these composite materials after excitation with α- (1) and β-particles (2) [24].

Therefore, composite materials capable to register simultaneously α- and β-radiation in mixed ionizing beams using the phenomenon of TL were developed. The developed epitaxial structures are the prototypes for constructing a new generation of composite TL detectors based on various oxide compounds crystallized using the LPE method.

4. Concluding remarks

The paper reviews three different approaches to development of CS and TL materials based on the garnet epitaxial structures for the simultaneous detection of particles and quanta in mixed ionizing beams. The **first approach** deals with choosing the dopants in a SCFs and a substrate of the same crystalline host, namely LuAG garnet, which provide different scintillation properties. The **second approach** is based on the use of various types of Ce^{3+} doped SCFs and crystals of mixed garnets, possessing different scintillation properties. The **third approach** is based on the difference in TL properties of SCFs and subastrate of simple or mixed garnets doped with Ce^{3+} ions.

The possibility of crystallizing $(Gd,Tb,Lu)_3(Al,Ga)_5O_{12}$:Ce SCFs of mixed garnets by the LPE growth method onto YAG and GAGG substrates was demonstrated using PbO and BaO fluxes. Such developed SCF scintillators can be used in microtomographic devices as scintillation screens with a very X-ray quanta absorption ability. At the same time, such SCF scintillators can be used also in monitoring of α- or/and β-particles in the mixed radiation fluxes.

Table 5 summarizes the developed CS and their scintillation properties.

Table 5. Comparison of scintillation properties of different composites materials based on garnet epitaxial structures.

Composite scintillator	The best ratio $t_{□}/t_{□}$	Intensity level for the best $t_{□}/t_{□}$ ratio	Optimal value of intensity	Time interval (ns)
LuAG:Pr SCF /LuAG:Ce SC	3.6	0.1	0.03-0.4	0-700
LuAG:Sc SCF /LuAG:Ce SC	2.2	0.05	0.05-0.2	200-900
LuAG:Ce SCF/LuAG:Pr SC	1.1	0.05	0.05-0.2	60-320
$Lu_{2.85}Tb_{0.15}$AG:Ce SCF/LuAG:Pr SC	1.2	0.05	0.1-0.02	200-1500
$Lu_{1.75}Tb_{0.3}$AG:Ce SCF/LuAG:Pr SC	1	-	-	-
$Lu_{1.35}Tb_{1.65}$AG:Ce SCF/LuAG:Pr SC	1.4	0.1	0.05-0.2	250-1000

$Lu_{0.715}Tb_{2.285}AG$:Ce SCF/LuAG:Pr SC	4.2	0.07	0.05-0.36	100-3000
LuAG:Ce SCF/ LuAG:Sc SC	2.7	0.05	0.02-0.2	250-110
LuAG:Pr SCF/ LuAG:Sc SC	15.6	0.05	0.01-0.5	0-2500
TbAG:Ce SCF/GAGG:Ce SC	3	0.05	0.05-0.2	450-3700
LGAGG:Ce SCF/GAGG:Ce SC	2	1/e	0.2 – 0.5	50-500
GAGG/GAGG	4.2	0.01	0.01 – 0.1	600-2700

CS based on SCFs and crystals of Ce^{3+} doped mixed garnets possess higher t_α/t_γ and higher LY in comparison with counterparts based on doped SCFs and crystals of LuAG garnet. LY in the developed TbAG:Ce and (Gd,Tb)(Al,Ga)O_{12}:Ce SCF scintillators is the highest among the known garnet SCFs obtained from PbO-based fluxes and show a very low afterglow level in the scintillation response. The highest t_α/t_γ ratio of up to 3 in the time interval of 450-3700 ns at the scintillation intensity decay level of 0.05 is registered in $Tb_3Al_5O_{12}$:Ce SCF/ $Gd_3Al_{2.5}Ga_{2.5}O_{12}$:Ce composite scintillator. The highest LY and the best separation of the decay curves under excitation by α-particles and γ-quanta among all the studied composition was achieved for $Gd_3Al_{5-x}Ga_xO_{12}$:Ce (x=1.15-2.67) SCF/GAGG2.5:Ce SC epitaxial structures, where the t_γ/t_α reached 4.2 in the 0-3000 ns time range at scintillation decay from 1/e to 0.01 levels. *This is the best scintillation figure-of-merit among all the developed types of CS based on SCFs and crystals of mixed garnets.* Therefore, such type of the developed CS can be successfully applied for simultaneous registration of α–, β-particles and γ-quanta in mixed radiation beams.

Prototypes of TL composite materials based on epitaxial structures of garnet compounds comprising SCFs and crystals of YAG:Ce and LuAG:Ce garnets were developed also using the LPE method. It has been shown that such composites can be used for detection of α- and β- particles using the differences between TL glow curves recorded from the SCFs and substrates. Among all the developed TL composite materials based on SCFs and crystals of garnet compounds, the most efficient registration of α- and β-particles is achieved with the YAG:Ce SCF/LuAG:Ce SC and $Lu_{1.5}Gd_{1.5}$AG:Ce SCF/YAG:Ce SC epitaxial structures where the temperature difference between the main TL peaks corresponding to the detection of α- and β- particles is equal to 165 and 215 ^oC, respectively.

Meanwhile, there is still a room for the development of the new types of CS and detectors with enhanced scintillation and TL properties. Such new types of composite detectors can be created on the base of materials with more suitable scintillation and TL characteristics in comparison with mentioned above garnet compounds. Namely, Lu_2SiO_5 (LSO) orthosilicate, $(Lu,Gd)_2Si_2O_5$ (LGPS) pyrosilicate, $LuAlO_3$ (LuAP) perovskite as well as $CdWO_4$ (CWO) tungstate hosts has significantly high density and effective atomic number in

comparison with Y, Lu and Gd based garnets [12, 43, 44]. For this reason, the Ce^{3+} doped LSO, LGPS and LuAP crystals as well as undoped CWO crystal are a very promising materials for producing the respective substrates at developed CS and detectors. The Ce^{3+} and Bi^{3+} doped SCFs of Y_2SiO_5 (YSO) orthosilicate, $(Y,Gd)_2Si_2O_{12}$ (YGdPS) pyrosilicate, $YAlO_3$ (YAP) and $GdAlO_3$ (GAP) perovskites and their solid solutions as well as Bi^{3+} doped CWO SCFs are also suitable compounds for the creation of film components of CS on their base [74-84].

Furthermore, the possibility of fabricating by the LPE method the advanced CS and TL detectors based on the films and crystals of all the above-mentioned oxide compounds needs technological and experimental conirmation. We plan to fabricate new types of CS and TL materials based on the SCF and single crystals of doped ortho- and pyrosilicates, perovskites and tungstates, with enhanced scintillation properties as compared to all well-known analogues, grown by the LPE method for the simultaneous registration of the different components of the mixed radiation beams.

Author Contributions: YZ – conceptualization, review and editing; SW – original draft preparation, PB, MN and AY – methodology; VG, TZ, YS and JAM – investigations; OS – review and editing.

Funding: This revive is based on the results performed in the frameworks of the Polish National Centre (NCN) 2016/21/B/ST8/03200 and 2018/31/B/ST8/03390 projects and partly 2017/25/B/ST8/02932 project. O. Sidletskiy acknowledges the scholarship of the Polish National Agency for Academic Exchange under agreement No. PPN/ULM/2020/1/00298/U/00001. O. Sidletskiy also thanks the "ENSEMBLE3 - Centre of Excellence for nanophotonics, advanced materials and novel crystal growth-based technologies" project (GA no. MAB/2020/14) carried out within the International Research Agendas programme of the Foundation for Polish Science cofinanced by the European Union under the European Regional Development Fund and the European Union's Horizon 2020 research and innovation programme Teaming for Excellence (GA no. 857543) for support of this work.

Acknowledgments: Authors acknowledges also to K. Paprocki from IP UKW; A. Fedorov from SSI Institute for Single Crystals, Kharkiv, I. Gerasymov, S. Tkachenko and P. Arhipov from ISMA Kharkiv, W. Gieszczyk, A. Mrozik and A. Twardak from INR PAN in Krakow; A. Beitlerova and R. Kucerkova from FZU, Prague as well as K. Kamada and S. Kurosawa from IMR Tohoku University, Sendai for their contribution as coauthors of the several papers mentioned in this review.

Conflicts of Interest: The authors declare no conflict of interest.

References

1. Zorenko, Yu.; Novosad, S.S.; Pashkovskii, M.V.; Lyskovich, A.B.; Savitskii, V.G.; Batenchuk, M.M.; Malyutenkov, P.S.; Patsagan, N.I.; Nazar and, I.V.; Gorbenko, V.I. Epitaxial structures of garnets as scintillation detectors of ionizing radiation. *J. Appl. Spectrosc.* **1990**, *52*, 645–649.

https://doi.org/10.1007/bf00662203 .

2. Ferrand, B.; Chambazand, B.; Couchaud, M. Liquid phase epitaxy: A versatile technique for the development of miniature optical components in single crystal dielectric media. *Opt. Mater*. **1999**, *11*, 101–114. https://doi.org/10.1016/S0925-3467(98)00037-8
3. Zazubovich, S.; Krasnikov, A.; Zorenko, Y.; Gorbenko, V.; Babin, V.; Mihokova, E.; Nikl, M. Nanocomposite, Ceramic, and Thin Film Scintillators, Publisher: Pan Stanford Publishing Pte. Ltd., 2016; pp. 227-305. ISBN: 978-981-4745-22-2
4. Robertson, J.M.; Van Tol, M.V. Cathodoluminescent garnet layers. *Thin Solid Films* **1984**, *114*, 221–240. https://doi.org/10.1109/TNS.2012.2188907
5. Hrytskiv, Z.D.; Zorenko, Y.; Gorbenko, V.; Pedanand, A.D.; Shkliarsyi, V.I. Single crystalline film screens for cathode-ray tubes: New life of television scanning optical microscopy. *Radiat. Meas.* **2007**, *42*, 933–936. https://doi.org/10.1016/j.radmeas.2007.02.043
6. Schauer, P.; Lalinský, O.; Kucera M. Overview of S(T)EM electron detectors with garnet scintillators: Some potentials and limits, *Microsc Res Tech*. **2021**, *84*, 753–770. https://doi.org/10.1002/jemt.23634
7. Molva, E.; Microchip lasers and their applications in optical microsystems. *Opt. Mater*. **1999**, *11*, 289–299. https://doi.org/10.1016/s0925-3467(98)00050-0
8. Klimczak, M.; Malinowski, M.; Sarnecki, J.; Piramidowicz, R.J. Luminescence properties in the visible of Dy:YAG/YAG planar waveguides. *Luminescence* **2009**, *129*, 1869–1873. https://doi.org/10.1016/j.jlumin.2009.04.073
9. Zorenko, Yu.; Batenchuk, M.; Gorbenko, V.; Pashkovsky, M. Single-crystalline oxide films of the Al2O3-Y2O3-R2O3 system as optical sensors of various types of ionizing radiation: significant advantages over volume analogs. *Proc. SPIE* **1997**, *2967*, 101. https://doi.org/10.1117/12.266516
10. Zorenko, Yu.; Gorbenko, V.; Konstankevych, I.; Grinevand, B.; Globus, M. Scintillation properties of Lu3Al5O12:Ce single-crystalline films. *Nucl. Instrum. Methods Phys. Res.* **2002**, *486*, 309–314. https://doi.org/10.1016/S0168-9002(02)00725-8
11. Koch, A.; Raven, C.; Spanne, P.; Snigirev, A. X-ray imaging with submicrometer resolution employing transparent luminescent screens. *J. Opt. Soc. Amer. A, Opt.* **1998**, *15*, 1940–1951. https://doi.org/10.1364/josaa.15.001940
12. Martin, T.; Koch, A. Recent developments in X-ray imaging with micrometer spatial resolution. *J. Synchrotron Radiat.* **2006**, *13*, 180–194. https://doi.org/10.1107/S0909049506000550
13. Zorenko, Y.; Gorbenko, V.; Konstankevych, I.; Pashkovsky, M.; Globus, M.; Grinyov, B.; Tarasov, V.; Dorenbos, P.; Van Eijk, C.; Van Loef, E. Scintillators on the base of single crystalline films of Al2O3-

Y2O3 system oxides. Proceedings of the 5th Intern. Conference on Inorganic Scintillators and Their Applications, Moscow State University, Moscow, 6-20.08.1999; Mikhailin, V.; Moscow, Moscow State University **2000**, 476-481. ISBN: 582790079

14. Globus, M.; Grinyov, B.; Ratner, M.; Tarasov, V.; Lyubinskiy, V.; Vydai, Yu.; Ananenko, A.; Zorenko, Yu.; Gorbenko, V.; Konstankevych, I. New type of scintillation detectors for biological, medical, and radiation monitoring applications. *IEEE Transactions on Nuclear Science* **2004**, *51*, 1297-1303. https://doi.org/10.1109/tns.2004.830113
15. Witkiewicz-Lukaszek, S.; Gorbenko, V.; Zorenko, T.; Paprocki, K.; Sidletskiy, O.; Gerasymov, I.; Mares, J.A.; Kucerkova, R.; Nikl, M.; Zorenko, Yu. Novel all-solid-state composite scintillators based on the epitaxial structures of LuAG garnet doped with Pr, Sc and Ce ions. *IEEE Transactions on Nuclear Science* **2018**, *65*, 2114 – 2119. https://doi.org/10.1109/TNS.2018.2838333
16. Witkiewicz-Lukaszek, S.; Gorbenko, V.; Zorenko, T.; Paprocki, K.; Sidletskiy, O.; Gerasymov, I.; Mares, J.A.; Kucerkova, R.; Nikl, M.; Zorenko, Yu. Composite scintillators based on the crystals and single crystalline films of LuAG garnet doped with Ce3+, Pr3+ and Sc3+ ions. *Optical Materials* **2018**, *84*, 593-599. https://doi.org/10.1016/j.optmat.2018.07.066 .
17. Mares, J.A.; Witkiewicz-Lukaszek, S.; Gorbenko, V.; Zorenko, T.; Kucerkova, R.; Beitlerova, A.; D′Ambrosio, C.; Dlouhy, J.; Nikl, M.; Zorenko, Yu. Alpha and gamma spectroscopy of Composite scintillators based on the LuAG:Pr crystals and single crystalline films of LuAG:Ce and (Lu,Gd,Tb)AG:Ce garnets. *Optical Materials* **2019**, 96, 109268. https://doi.org/10.1016/j.optmat.2019.109268
18. Witkiewicz-Lukaszek, S.; Gorbenko, V; T. Zorenko, O. Sidletskiy, P. Arhipov, A. Fedorov, J.A. Mares, R. Kucerkova, M. Nikl, Yu. Zorenko. Liquid phase epitaxy growth of high-performance composite scintillators based on single crystalline films and crystals of LuAG. *CrystEngComm*, **2020**, *22*, 3713-3724. https://dpi.org/10.1039/D0CE00266F.
19. Gorbenko, V.; Witkiewicz-Lukaszek, S.; Zorenko, T.; Syrotych, Y.; Mares, J.A.; Kucerkova, R.; Nikl, M.; Sidletskiy, O.; Fedorov, A.; Zorenko. Yu. Development of composite scintillators based on the LuAG:Pr single crystalline films FILMS and LuAG:Sc single crystals, Crystals, 2021, 11(8), 846; https://doi.org/10.3390/cryst11080846.
20. S. Witkiewicz-Lukaszek, V. Gorbenko, T. Zorenko, O. Sidletskiy, I. Gerasymov, A. Fedorov, A. Yoshikawa, J. A. Mares, M. Nikl, and Yu. Zorenko, Development of composite scintillators Based on single crystalline films and Crystals of Ce3+-Doped (Lu,Gd)3(Al, Ga)5O12 Mixed Garnet Compounds, *Crystal Growth & Design*, **2018,** 18 (3), 1834–1842; https://doi.org/10.1021/acs.cgd.7b01695.
21. Witkiewicz-Lukaszek, S.; Gorbenko, V.; Zorenko, T.; Paprocki, K.; Sidletskiy, O.; Fedorov, A.; Kucerkova, R.; Mares, J.A.; Nikl, M.; Zorenko, Yu. Epitaxial growth of composite scintillators based on

Tb3Al5O12:Ce single crystalline films and Gd3Al2.5Ga2.5O12:Ce crystal substrates. *CrystEngComm*, **2018**, *20*, 3994-4002 https://doi.org/10.1039/C8CE00536B .

22. Witkiewicz-Lukaszek, S.; Gorbenko V.; Zorenko, T.; Syrotych, Y., Kucerkova, R.; Mares, J.A.; Nikl, M.; Sidletskiy, O.; Fedorov, A.; Kurosawa, S., Kamada, K.; Yoshikawa, A.; Zorenko, Y. New types of composite scintillators based on the single crystalline films and crystals of Gd3(Al,Ga)5O12:Ce mixed garnets. *Materials Science & Engineering B* **2021**, *264*, 114909. https://doi.org/10.1016/j.mseb.2020.114909
23. Witkiewicz-Lukaszek, S.; Gorbenko, V.; Bilski, P.; Mrozik, A.; Zorenko, T.; Fedorov, A.; Zorenko, Y. LPE growth of composite thermoluminescent detectors based on the Lu3−xGdxAl5O12: single crystalline films and YAG:Ce crystals. *Crystals* **2020**, 10, 189. https://doi.org/10.3390/cryst10030189 .
24. Witkiewicz-Lukaszek, S.; Gorbenko, V.; Zorenko, T.; Zorenko, Y.; Gieszczyk, W.; Mrozik, A.; Bilski, P. Composite thermoluminescent detectors based on the Ce3+ doped LuAG/YAG and YAG/LuAG epitaxial structures. *Radiation Measurements* **2019**, *128*, 106124. https://doi.org/10.1016/j.radmeas.2019.106124
25. Zorenko, Yu.; Gorbenko, V.; Savchyn, V.; Fedorov, A.; Kuklinski, B.; Grinberg, M.; Bilski, P.; Gieszczyk, W.; Twardak, A.; Mandowski, A.; Mandowska, E. Luminescent properties of YAlO3:Mn single crystalline films, *Optical Materials*, **2012,** 34, 1979-1983. https://doi.org/10.1016/j.optmat.2011.12.003
26. Gieszczyk, W.; Bilski, P.; Kłosowski, M.; Mrozik, A.; Zorenko, Yu.; Zorenko**,** T.; Paprocki, K.. Luminescent properties of undoped and Ce3+ doped crystals in Y2O3–Lu2O3-Al2O3 triple oxide system grown by micro-pulling-down method. *Optical Materials*, **2019,** 89, 408–413. https://doi.org/10.1016/j.optmat.2019.01.023 .
27. Zorenko, Yu.; V. Gorbenko, V.; Growth peculiarities of the R3Al5O12 (R= Lu, Yb, Tb, Eu-Y) single crystalline film phosphors by Liquid Phase Epitaxy. *Radiation Measurements*. **2007**, 42, 907-910; https://doi.org/10.1016/j.radmeas.2007.02.049
28. Gorbenko, V.; Zorenko, T.; Pawlowski, P.; Iskaliyeva, A.; Paprocki, K.; Suchocki, A.; Zhydachevskii, Ya.; Fedorov, A.; Khaidukov, N.; Van Deun, R.; Schröppel, F.; Osvet, A.; Batentschuk, M.; Zorenko, Yu. Luminescent and scintillation properties of Ce3+ doped Ca2RMgScSi3O12 (R=Y, Lu) single crystalline films, *Journal of Luminescence*, **2018,** 195, 362-370; https://doi.org/10.1016/j.jlumin.2017.11.052
29. Zorenko, Y.; Gorbenko, V.; Witkiewicz, S.; Zorenko, Yu. Luminescent properties of (La,Lu,Gd)3(Al,Sc,Ga)5O12:Ce mixed garnets under synchrotron radiation excitation, Journal of Luminescence, 2018, 199, 483-487. https://doi.org/10.1016/J.JLUMIN.2018.03.093
30. Chen, R.; Pagonis, V. (Eds), Advances in Physics and Applications of Optically and Thermally Stimulated Luminescence, World Scientific (2019) 285-317. https://doi.org/10.1142/q0172
31. Yukihara, E.; Kron, T. Thermoluminescence dosimetry (TLD) in medicine: five ‘w’s and one how. *Rad. Prot. Dosim*., 192, **2020**, 139–151. https://doi.org/10.1093/rpd/ncaa212

32. Bilski, P. Lithium Fluoride: from LiF:Mg,Ti to LiF:Mg,Cu,P. *Radiat Prot Dosim*. 100, 2002, 199-203. https://doi.org/10.1093/oxfordjournals.rpd.a005847

33. Horowitz, Y. S. Thermoluminescence dosimetry: State-of-the-art and frontiers of future research. *Radiat Meas*. 71, **2014**, 2-7. https://doi.org/10.1016/j.radmeas.2014.01.002

34. Bilski, P.; Olko, P.; Burgkhardt, B.; Piesch, E. Ultra-Thin LiF:Mg,Cu,P Detectors for Beta Dosimetry. *Radiat Meas.* 24, **1995**, 439-443. https://doi.org/10.1016/1350-4487(94)00125-K

35. Bilski, P.; Budzanowski, M.; Olko, P.; Christensen, P. Properties of Different Thin-Layer LiF:Mg,Cu,P TL Detectors for Beta Dosimetry. *Radiat Prot Dosim*. 66, **1996**, 101-104. https://doi.org/10.1093/oxfordjournals.rpd.a031693

36. Bueno, M.; Carrasco, P.; Jornet, N.; Munoz-Montplet, C.; Duch, M. A. On the suitability of ultrathin detectors for absorbed dose assessment in the presence of high-density heterogeneities. *Medical Physics*. 41,**2014**, 142-153. https://doi.org/10.1118/1.4886760

37. Grassi, E.; Sghedoni, R.; Piccagli, V.; Fioroni, F.; Borasi, G.; Iori, M. Comparison of two different types of LiF:Mg,Cu,P thermoluminescent dosimeters for detection of beta rays (beta-TLDs) from Sr-90/Y-90, K-85 and Pm-147 sources. *Health Physics.* 100, **2011**, 515-522. https://doi.org/0.1097/HP.0b013e3182092732

38. Goksu, H. Y.; Bulur, E.; Wahl, W. Beta dosimetry using thin-layer alpha-Al2O3:C TL detectors. *Rad Prot Dosim.* 84, **1999**, 451-455. https://doi.org/10.1093/oxfordjournals.rpd.a032775

39. Twardak, A.; Bilski, P.; Zorenko, Y.; Gorbenko, V.; Mandowski, A.; Mandowska, E.; Sidletskiy, O. Comparative study of TSL and OSL properties of LSO and LSO:Ce single crystals and single crystalline films, *Radiation Measurements*, **2013,** 56, 196-199. https://doi.org/ 10.1016/j.radmeas.2013.01.063

40. Nikl, M.; Tous, T.; Mares, J.A.; Prusa, P.; Mihokova, E.; Blazek, K.; Vedda, A.; Zorenko, Yu.; Gorbenko, V.; Babin, V. Lu3Al5O12-based materials for high 2D-resolution scintillation detectors. *Proc. SPIE* **2009**, *7310*, 731008. https://doi.org/10.1117/12.818358 .

41. Nikl, M.; Yoshikawa, A.; Kamada, K.; Stanek, C.R.; Blazek, K. Development of LuAG-based scintillator crystals – A review, Progress in Crystal Growth and Characterization of Materials, **2013,** 59, 47-72, https://doi.org/10.1016/j.pcrysgrow.2013.02.001.

42. Kamada, K.; Yanagida, T.; Pejchal, J.; Nikl, M.; Endo, T.; Tsutsumi, K.; Fujimoto, Y.; Fukabori, A.; Yoshikawa, A. Crystal growth and scintillation properties of Ce doped Gd3Al2Ga3O12 single crystals. *IEEE Trans. Nucl. Sci.* **2012**, *59*, 2112–2115. https://doi.org/10.1109/TNS.2012.2197024.

43. Crytur. Integrated crystal based solutions. Available online: www.crytur.cz (24.11.2021)

44. Advatech – Radiation Detection/Imaging and Photonics. Available online: www.advatech-uk.co.uk (24.11.2021)

45. Vrubel, I.; Polozkov, R.; Shelykh, I.; Khanin, V.; Rodnyi, P.; and Ronda C. Bandgap Engineering in Yttrium−Aluminum Garnet with Ga Doping, *Cryst. Growth Des.* **2017**, *17*, 4, 1863–1869; https://doi.org/10.1021/acs.cgd.6b01822

46. Li, M.; Meng, M.; Chen, J.; Sun, Y.; Cheng, G.; Chen, L.; Zhao, S.; Wan, B; Feng, H.; Ren, G.; and Ding, D. Abnormal Site Preference of Al and Ga in Gd3Al2.3Ga2.7O12:Ce, *Phys. Status Solidi B* **2021**, 2000603; https://doi.org/10.1002/pssb.202000603

47. Nargelas, S; Talochka, Y.; Vaitkevicius, A., Dosovitskiy, G., Buzanov, O., Vasil'ev, A., Malinauskas, T., Korzhik, M., Tamulaitis, G. Influence of matrix composition and its fluctuations on excitation relaxation and emission spectrum of Ce ions in (GdxY1-x)3 Al2Ga3O12:Ce scintillators, *J. Lumin.* **2022**, *242*, 118590. https://doi.org/10.1016/j.jlumin.2021.118590

48. Khanin, V.; Venevtsev, I.; Chernenko, K.; Pankratov, V.; Klementiev, K.; van Swieten, T.; van Bunningen, A.J.; Vrubel, I.; Shendrik, R.; Ronda, C.; Rodnyi, P.; Meijerink, A. Exciton interaction with Ce3+ and Ce4+ ions in (LuGd)3(Ga,Al)5O12 ceramics, *J. Lumin.* **2021**, *237*, 118150. https://doi.org/10.1016/j.jlumin.2021.118150

49. Korzhik, M.; Alenkov, V.; Buzanov, O.; Dosovitskiy, G.; Fedorov, A.; Kozlov, D.; Mechinsky, V.; Nargelas, S.; Tamulaitis, G.; Vaitkevičius, A. Engineering of a new single-crystal multi-ionic fast and high-light-yield scintillation material (Gd0.5–Y0.5)3Al2Ga3O12:Ce,Mg, *CrystEngCom*m, **2020**, *22*, 2502–2506. https://doi.org/10.1039/d0ce00105h

50. Pankratova V.; Kozlova, A.; Buzanov, O.; Chernenko, K.; Shendrik, R.; Šarakovskis, A. , Pankratov, V. Time-resolved luminescence and excitation spectroscopy of Co-doped Gd3Ga3Al2O12 scintillating crystals. *Sci. Rep.* **2020** *10*, 20388. https://doi.org/10.1038/s41598-020-77451-x.

51. Dantelle, G.; Boulon, G.; Guyot, Y.; Testemale, D.; Guzik, M.; Kurosawa, S.; Kamada, K. and Yoshikawa A. Research on Efficient Fast Scintillators: Evidence and X-Ray Absorption Near Edge Spectroscopy Characterization of Ce4+ in Ce3+, Mg2+-Co-Doped Gd3Al2Ga3O12 Garnet Crystal, *Phys. Status Solidi B* **2019**, 1900510; https://doi.org/10.1002/pssb.201900510

52. Bárta, J.; Pestovich, K.S.; Valdez, J.A.; Wiggins, B.W.; Richards, C.; Smith, E.; Clayton, J.H.; Smalley, D.; McClellan, K.J. Compositional screening of Ce-doped (Gd,Lu,Y)3(Al,Ga)5O12 ceramics prepared by quenching from melt and their luminescence properties, *J. Alloys Comp.* **2021**, *889*, 161687. https://doi.org/10.1016/j.jallcom.2021.161687

53. Nakauchi, D.; Okada G.; Kawano, N.; Kawaguchi, N.; and Yanagida, T. Effects of Ga substitution in Ce:Tb3GaxAl5%xO12 single crystals for scintillator applications, *Jap. J. Appl. Phys.* **2018**, *57*, 02CB02. https://doi.org/10.7567/JJAP.57.02CB02

54. Boyarintseva, Y.; Neicheva, S.; Zhmurin, P.; Arhipov, P.; Gerasymov, Ia.; Tkachenko, S.; Sidletskiy, O.; Baumer, V.; Vovk, O.; Nizhankovskyi, S. Optical study of Y3-xGdxAl5O12:Ce crystals grown from the melt, *Opt. Mater*., **2019**, *96*, 109283. https://doi.org/10.1016/j.optmat.2019.109283

55. Gerasymov, Ia.; Nepokupnaya, T.; Boyarintsev, A.; Sidletskiy, O.; Kurtsev, D.; Voloshyna, O.; Trubaieva, O.; Boyarintseva, Y.; Sibilieva, T.; Shaposhnyk, A.; Opolonin, O.; Tretyak, S. GAGG:Ce composite scintillator for X-ray imaging, *Opt. Mater.* **2020**, *109*, 110305. https://doi.org/10.1016/j.optmat.2020.110305

56. Nikl, M.; Mihokova, E.; Pejchal, J.; Vedda, A.; Zorenko, Yu.; Nejezchleb, K. The antisite LuAl defect-related trap in Lu3Al5O12:Ce single crystal. *Phys. Stat. Sol. (b)*, **2005**, 242, 119-121. https://doi.org/10.1002/pssb.200541225

57. Fasoli, M.; A. Vedda, A; M. Nikl, M.; Jiang, C.; Uberuaga, B., Andersson, D., McClellan, K.; C. Stanek, C. Band-gap engineering for removing shallow traps in rare-earth Lu3Al5O12 garnet scintillators using Ga3+ doping. *Phys. Rev. B* 2011, 84, 081102(R). https://doi.org/10.1103/PhysRevB.84.081102

58. Nikl, M.; Yoshikawa, A. Recent R&D Trends in Inorganic Single-Crystal Scintillator Materials for Radiation Detection. Advanced Optical Materials, 2015, 3, 463-481. https://doi.org/10.1002/adom.201400571

59. Zorenko, Yu.; Gorbenko, V.; Savchyn, V.; Zorenko, T.; Fedorov, A.; Wrzesiński, H.; Vasylkiv, Ya. Multi-component Ce doped (Gd,Y,La,Lu)3(Al,Ga,Sc)5O12 garnets - a new story in the development of scintillating single crystalline film screens, Radiation Measurements, **2013,** 56, 150-154. https://doi.org/10.1016/j.radmeas.2013.03.011

60. Zorenko, Yu.; Gorbenko, V.; Savchyn, V.; Zorenko, T.; Fedorov, A.; Sidletskiy, O. Development of scintillating screens based on the SINGLE CRYSTALLINE FILMS of Ce doped (Gd,Y)3(Al,Ga,Sc)5O12 multicomponent garnets, *Journal of Crystal Growth*, **2014**, 401, 532-536; https://doi.org/10.1016/j.jcrysgro.2014.01.075

61. Prusa, P.; Kucera, M.; Mares, J.A.; Hanus, M.; Beitlerova, A.; Onderisinova, Z.; Nikl, M. Scintillation properties of the Ce-doped multicomponent garnet epitaxial films. *Optical Materials*, **2013**, 35, 2444-2448, https://doi.org/10.1016/j.optmat.2013.06.051

62. Zorenko, Yu.; Gorbenko, V.; Vasylkiv, Ja.; Zelenyj, A.; Fedorov, A.; Kucerkova, R.; Mares, J.A.; Nikl, M.; Bilski, P.; Twardak, A. Growth and luminescent properties of scintillators based on the single crystalline films of Lu3−xGdxAl5O12:Ce garnet. Material Research Bulletin, **2015,** 64, 355–363. https://doi.org/10.1016/j.materresbull.2015.01.020

63. Zorenko, Yu.; Gorbenko, V.; Vasylkiv, Ja.; Strzyzewski, T.; Fedorov, A.; Kucerkova, R.; Mares, J.A.; Nikl, M.; Bilski, P.; Twardak, A. Growth and luminescent properties of scintillators based on the single

crystalline films of (Lu,Gd)3(Al,Ga)5O12:Ce garnets. *J. Lumin.* **2016**, *169*, 828–837, https://doi.org/10.1016/j.materresbull.2015.01.020

64. Zorenko, Yu.; Gorbenko, V.; Zorenko, T.; Sidletskiy, O.; Fedorov, A.; Bilski, P.; Twardak, A.; Bilski, P. High-perfomance Ce-doped multicomponent garnet single crystalline film scintillators. *Phys. Status Solidi RRL*, **2015**, 9, 489-493. https://doi.org/10.1002/pssr.201510225
65. Prusa, P.; Kucera, M.; Mares, J.A.; Onderisinova, Z.; Hanus, M.; Babin, V.; Beitlerova, A.; Nikl, M. Composition Tailoring in Ce-Doped Multicomponent Garnet Epitaxial Film Scintillators. *Cryst. Growth Des.* **2015**, *15*, 3715-3723. https://doi.org/10.1021/acs.cgd. 5b00309
66. Zorenko, Y.; Gorbenko V.; Zorenko, T.; Paprocki, K.; Nikl, M.; Mares, J.A.; Bilski, P.; Twardak, A.; Sidletskiy, O.; Gerasymov, I.; Grinyov, B.; Fedorov, A. Scintillating screens based on the single crystalline films of multicomponent garnets: New achievements and possibilities. *IEEE Transactions on Nuclear Science* **2016**, *63*, 497-502. https://doi.org/10.1109/TNS.2015.2514062
67. Zorenko, Y.; Gorbenko, V.; Zorenko, T.; Paprocki, K.; Bilski, P.; Twardak, A.; Voznyak, T.; Sidletskiy, O.; Gerasimov, Y.; Gryniov, B.; Fedorov, A. Composition engineering of single crystalline films based on the multicomponent garnet compounds. *Optical Materials* **2016**, *61*, 3-10. https://doi.org/10.1016/j.optmat.2016.03.031
68. Zorenko, Y.; Douissard, P.; Martin, T.; Riva, F.; Gorbenko, V.; Zorenko, T.; Paprocki, K.; Iskalieva, A.; Witkiewicz, S.; Fedorov, A.; Bilski, P.; Twardak, A. Scintillating screens based on the LPE grown Tb3Al5O12:Ce single crystalline films. *Optical Materials* **2017**, *65*, 73-81. https://doi.org/10.1016/j.optmat.2016.09.066
69. Gorbenko, V.; Zorenko, T.; Witkiewicz, S.; Paprocki, K.; Sidletskiy, O.; Fedorov, A.; Bilski, P.; Twardak, A.; Zorenko, Y. LPE growth of single crystalline film scintillators based on Ce3+ Doped Tb3−xGdxAl5−yGayO12 mixed garnets. *Crystals* **2017**, 7(9), 262. https://doi.org/10.3390/cryst7090262
70. Babin, P. Herman, M. Kucera, M. Nikl, S. Zazubovich. Effect of Mg2+ co-doping on the photo- and thermally stimulated luminescence of the (Lu,Gd)3(Ga,Al)5O12:Ce epitaxial films. Journal of Luminescence, 215 (2019) 116608. https://doi.org/10.1016/j.jlumin.2019.116608
71. Lalinsky O.; Schauer, P.; and Kucera M. Influence of Mg-to-Ce Concentration Ratio on Cathodoluminescence in LuAG and LuGAGG Single-Crystalline Films, *Phys. Status Solidi A* **2019**, *216*, 1801016. https://doi.org/10.1002/pssa.201801016
72. Prusa, P.; Kučera, M.; Babin, V.; Bruza, P.; Parkman, T.; Panek, D.; Beitlerova, A.; Mares, J.A.; Hanus, M.; Lučeničová, Z.; Pokorny, M.; Nikl, M. Tailoring and Optimization of LuAG:Ce Epitaxial Film Scintillation Properties by Mg Co-Doping. *Crystal Growth and Design*, **2018**, *18*, 4998–5007. https://doi.org/10.1021/acs.cgd.8b00411

73. Schauer, P.; Lalinský, O.; Kučera, M.; Lučeničová, Z.; Hanuš, M. Effect of Mg co-doping on cathodoluminescence properties of LuGAGG:Ce single crystalline garnet films. *Optical Materials* **2017**, *72*, 359-366. https://doi.org/10.1016/j.optmat.2017.06.028

74. Babin, V.; Boháček, P.; Jurek, K.; Kučera, M.; Nikl, M.; Zazubovich, S. Dependence of Ce3+ - related photo- and thermally stimulated luminescence characteristics on Mg2+ content in single crystals and epitaxial films of Gd3(Ga,Al)5O12:Ce,Mg. *Optical Materials* **2017**, *83*, 290-299. https://doi.org/10.1016/j.optmat.2018.05.087

75. Zorenko, Yu.; Gorbenko, V.; Savchyn, V.; Zorenko, T.; Grinyov, B.; Sidletskiy, O.; Fedorov, A. Growth and luminescent properties of Ce and Ce-Tb doped (Y,Lu,Gd)2SiO5:Ce SINGLE CRYSTALLINE FILMS, *Journal of Crystal Growth*, **2014,** 401, 577–583.

76. Zorenko, Yu.; Gorbenko, V.; Zorenko, T.; Malinowski, P.; Jary, V., Kucerkova, R.; Beitlerova, A.; Mares, J.A.; Nikl, M.; Fedorov, A. Luminescent and scintillation properties of Bi3+ doped Y2SiO5 and Lu2SiO5 single crystalline films. *Journal of Luminescence,* **2014,** 154, 525-530. https://doi.org/10.1016/j.jlumin.2014.05.030

77. Kilian, A.; Bilski, P.; Gorbenko, V.; Zorenko, T.; Witkiewicz, S.; Paprocki, K.; Zorenko, Yu. Thermoluminescent properties of cerium doped Lu2SO5 and Y2SiO5 single crystalline films grown from PbO-B2O3 and Bi2O3 fluxes, Crystals, **2018,** 8, 120(12); https://doi.org/10.3390/cryst8030120 .

78. Kurosawa, S.; Yoshikawa, A.; Gorbenko, V.; Zorenko, T.; Witkiewicz-Lukaszek, S.; Zorenko, Yu. Composite scintillators based on the films and crystals of (Lu,Gd,La)2Si2O7 pyrosilicates. *IEEE Transactions on Nuclear Science*, 2020, 67, 994 – 998, https://doi.org/10.1109/TNS.2020.2983657.

79. Zorenko, Y.; Gorbenko, V., Konstankevych, I.; Voznjak, T.; Savchyn, V.; Nikl, M.; Mares, J.A.; Nejezchleb, K.; Mikhailin, V.; Kolobanov, V.; Spassky; D. Peculiarities of luminescence and scintillation properties of YAP:Ce and LuAP:Ce single crystals and single crystalline films. Radiation Measurements, **2007,** 42, 528-532; https://doi.org/10.1016/j.radmeas.2007.01.046.

80. Zorenko, Yu., Gorbenko, V., Zorenko, T., Voznyak, T.; Riva, F., Douissard, P.A.; Martin, T.; Fedorov, A.; Suchocki, A.; Zhydachevski, Ya. Growth and luminescent properties of single crystalline films of Ce3+ doped Pr1-xLuxAlO3 and Gd1-xLuxAlO3 perovskites, *Journal of Crystal Growth*, **2017,** 457, 220-226. https://doi.org/10.1016/j.jcrysgro.2016.02.020

81. Riva, F.; Douissard, P-.A.; Martin, T.; Carla, F.; Zorenko, Y.V.; Dujardin, C. Epitaxial growth of gadolinium and lutetium-based aluminum perovskites thin film for X-rays micro-imaging applications, CrystEngComm, **2016,** 608–615; https://doi.org/10.1039/C5CE01938A.

82. Gorbenko, V., Zorenko, T., Paprocki, K.; Riva, F.; Douissard, P.A.; Martin, T.; Zhydachevskii, Y.; Suchocki, A.; Fedorov, A.; Zorenko, Yu. Epitaxial growth of the single crystalline films scintillating screens

based on the Eu3+ doped RAlO3 (R= Y, Lu, Gd, Tb) perovskites. *CrystEngComm*, **2018,** 20, 937-945, https://doi.org/10.1039/C7CE02074K

83. Zorenko, Yu.V. Luminescence of the mercury-like impurities in the $CdWO_4$ single-crystalline compounds. *Journal of Applied Spectroscopy*. **1998,** 65, 211-215; https://doi.org/10.1007/BF02680472.

84. Zorenko, Yu., Gorbenko, V., Voznyak, T., Konstankevych, I., Savchyn, V., Batentschuk, M.; Winnacker, A.; Brabec, Ch. Scintillators based on CdWO4 and CdWO4:Bi single crystalline films. IEEE Trans. Nucl. Sci. **2012,** 59, 2281-2285; https://doi.org/10.1109/TNS.2012.2201171.